J. Fluid Mech. (2002), *vol.* 460, *pp.* 1–38.
DOI: 10.1017/S0022112001006607 Printed in the United Kingdom

A spectral study of differential diffusion of passive scalars in isotropic turbulence

By MARK ULITSKY[1], T. VAITHIANATHAN[2] AND LANCE R. COLLINS[2]†

[1]Group T–3, MS B216, Los Alamos National Laboratory, Los Alamos, NM 87545, USA

[2]Department of Chemical Engineering, The Pennsylvania State University, University Park, PA 16802, USA

(Received 28 June 2000 and in revised form 26 July 2001)

In a companion paper, Ulitsky & Collins (2000) applied the eddy-damped quasi-normal Markovian (EDQNM) turbulence theory to the mixing of two inert passive scalars with different diffusivities in stationary isotropic turbulence. Their paper showed that a rigorous application of the EDQNM approximation leads to a scalar covariance spectrum that violates the Cauchy–Schwartz inequality over a range of wavenumbers. The violation results from the improper functionality of the inverse diffusive time scales that arise from the Markovianization of the time evolution of the triple correlations. The modified inverse time scale they proposed eliminates this problem and allows meaningful predictions of the scalar covariance spectrum both with and without a uniform mean gradient.

This study uses the modified EDQNM model to investigate the spectral dynamics of differential diffusion. Consistent with recent DNS results by Yeung (1996), we observe that whereas spectral transfer is predominantly from low to high wavenumbers, spectral incoherence, being of molecular origin, originates at high wavenumbers and is transferred in the opposite direction by the advective terms. Quantitative comparisons between the EDQNM model and the DNS show good agreement. In addition, the model is shown to give excellent estimates for the dissipation coefficient defined by Yeung (1998).

We show that the EDQNM scalar covariance spectrum for two scalars with different molecular diffusivities can be approximated by the EDQNM autocorrelation spectrum for a scalar with molecular diffusivity equal to the arithmetic mean of the first two scalars. The result is exact for the case of an isotropic scalar and is shown to be a very good approximation for the scalar with a uniform mean gradient. We then exploit this relationship to derive a simple formula for the correlation coefficient of two differentially diffusing scalars as a function of their two Schmidt numbers and the turbulent Reynolds number. A comparison of the formula with the EDQNM model shows the model predicts the correct Reynolds number scaling and qualitatively predicts the dependence on the Schmidt numbers.

To investigate the degree of local versus non-local transfer of the scalar covariance spectrum, we divided the energy spectrum into three ranges corresponding to the energy-containing eddies, the inertial range, and the dissipation range. Then, by conditioning the scalar transfer on the energy contained within each of the three ranges, we have determined that the transfer process is dominated first by local

† Author to whom correspondence should be addressed. Present address: Sibley School of Mechanical and Aerospace Engineering, Cornell University, 246 Upson Hall, Ithaca, NY 14853, USA.

interactions (local transfer) followed by non-local interactions leading to local transfer. Non-local interactions leading to non-local transfer are found to be significant at the higher wavenumbers. This result has important implications for defining simpler spectral models that potentially can be applied to more complex engineering flows.

1. Introduction

Models of non-premixed flames often make the assumption that the molecular and thermal diffusivities of all of the reacting species are equal. This simplification, referred to in the literature as the unity Lewis number assumption, is extremely attractive. It ultimately leads to a Shvab–Zeldovich conserved scalar formulation (Williams 1985) that reduces the calculation of species concentrations in the flame to that of a single scalar (the mixture fraction), regardless of the complexity of the chemistry or the number of species. However, there is growing experimental evidence (Bilger & Dibble 1982; Drake, Pitz & Lapp 1986; Kerstein *et al.* 1989; Chen, Bilger & Dibble 1990; Vranos *et al.* 1992) that so-called differential diffusion may be important at low-to-moderate Reynolds numbers. Differential diffusion refers to effects associated with differences in the molecular diffusivities of the reacting species. Unfortunately, differential diffusion cannot be captured by the conserved scalar approximation, and therefore we must resort to a full description of all of the reacting species to properly account for this phenomenon.

Initial studies of differential diffusion focused primarily on the decorrelation of inert passive scalars. Experiments (Kerstein *et al.* 1989; Smith *et al.* 1995*a*; Saylor & Sreenivasan 1998) and direct numerical simulations (Yeung & Pope 1993; Yeung 1996; Nilsen & Kosály 1997) found that differential diffusion, being of molecular origin, is initiated at high wavenumbers. Owing to an inverse cascade of 'incoherence,' however, it is ultimately manifested at lower wavenumbers. Yeung (1996) used DNS to investigate the detailed behaviour of the different classes of triadic interactions that are responsible for the inverse cascade of incoherence. Previously, this type of spectral analysis of the transfer process had only been applied to the Navier–Stokes equations (Domaradzki & Rogallo 1990; Zhou 1993*a*,*b*; Brasseur & Wei 1994). Yeung (1996) observed that transfer of the covariance spectrum was dominated by local transfer, although non-local interactions were significant.

Another important question addressed by these studies is how differential diffusion scales with Reynolds number. The argument is often made that at high Reynolds numbers, molecular effects are confined to high wavenumbers and thus have a small effect on single-point quantities of interest. Kerstein, Cremer & McMurtry (1995) proposed that the variance of the relative scalar fluctuation should scale like $Re_L^{-1/2}$, where Re_L is the Reynolds number based on the integral length scale. This hypothesis was corroborated by the DNS study of Nilsen & Kosály (1997).

Differential diffusion in reacting flows shows a similar phenomenology (Smith *et al.* 1995*b*; Jaberi *et al.* 1997; Nilsen & Kosály 1999), although it appears that reactions increase the magnitude of the effect. This is most probably due to an increase in scalar gradients that accompanies depletion of the reactant species. However, one puzzling result that has yet to be fully explained is the Reynolds number scaling observed by Smith *et al.* (1995*b*). In contrast to the mixing study by the same authors (Smith *et al.* 1995*a*), the reacting jet did not show a lessening of differential diffusion with increasing Reynolds number. This suggests that there may be something fundamentally different about the reacting system that is not captured by the inert studies.

The most popular models of non-premixed flames are based on a probability density function (p.d.f.) of the scalar species and temperature (Pope 1985; Girimaji 1991, 1992; Fox 1992). The strength of the p.d.f. model lies in its exact treatment of advection and of the highly nonlinear reaction terms. However, the p.d.f. has difficulty describing differential diffusion because the diffusive terms in the p.d.f. equations are modelled. Moreover, as differential diffusion is predominantly a small-scale phenomenon, it is difficult for a single-point description such as the p.d.f. to capture this effect.

In contrast, spectral models are inherently capable of describing differential diffusion accurately, since it is advection that is modelled whereas diffusion is treated exactly. Fox (1992) recently extended the Lagrangian spectral relaxation model (Fox 1995, 1997) to treat differential diffusion of non-reacting scalars. The model was able to reproduce several of the features found in the unpublished DNS by Yeung. The alternative approach taken in this study is based on the EDQNM (eddy damped quasi-normal Markovian) theory. The EDQNM theory was developed by Orszag (1970) as a correction to the quasi-normal approximation of Millionshtchikov (1941) that was shown to yield unrealizable spectra (O'Brien & Francis 1962; Ogura 1963). The theory has proved to be effective for investigating turbulent energy spectra (André & Lesieur 1977; Lesieur 1987) and passive scalar spectra (Vignon & Cambon 1980; Herring *et al.* 1982; Nakauchi, Oshima & Saito 1989; Herr, Wang & Collins 1996). In a companion study (Ulitsky & Collins 2000 hereinafter referred to as UC), the EDQNM model was derived for the scalar covariance spectrum for two scalars with different molecular diffusivities both with and without a uniform mean gradient. The main result of that work was that a straightforward application of the EDQNM theory produces a model for the scalar covariance spectrum that does not satisfy the Cauchy–Schwartz inequality over a range of wavenumbers. Upon further investigation, it was found that the problem originates with the inverse diffusive time scales in the triple correlations after Markovianization. UC modified these inverse time scales so that they were no longer explicit functions of the scalar molecular diffusivities. The modified EDQNM model for the isotropic scalars was shown to be realizable via a Langevin equation analysis, while the modified model for the anisotropic scalars produced realizable results for all time and for all values of the parameters attempted.

In the present study, we apply the modified EDQNM model to differentially diffusing, inert passive scalars. The investigation is similar to the one by Yeung (1996), except that we use a spectral model in place of DNS. An important advantage of the model is that it involves only averaged quantities, and thus eliminates the statistical noise associated with DNS and simplifies the interpretation of the results. Section 2 gives a summary of the modified EDQNM model, which is then compared to DNS in § 3. Section 4 explores a simplified model for the scalar covariance spectrum when the ratio of the Schmidt numbers is within an order of magnitude. The result is used to derive a simple formula for the correlation coefficient. Section 5 discusses the Reynolds number scaling of differential diffusion. We show that several single-point and spectral quantities can be collapsed when plotted in the appropriate coordinates. In § 6, we determine whether the advective transfer process is governed by local or non-local triadic interactions and whether the overall transfer process is local or non-local. The answers to these questions have important implications for constructing simpler and more flexible spectral models that can be more easily extended to inhomogeneous flows. Finally, the findings of the study are summarized in § 7.

2. EDQNM model equations

A complete development of the EDQNM model equations can be found in UC; thus, here, we simply present the equations. We consider the advection and diffusion of two (or more) passive scalars by isotropic turbulence. For the sake of simplicity, we restrict our attention to velocity fields that are mirror-symmetric or equivalently helicity free (an in-depth discussion on helicity in turbulence can be found in Lesieur 1987). The equation governing each scalar is given by

$$\frac{\partial \phi_\alpha}{\partial t} + \frac{\partial}{\partial x_i}(u_i \phi_\alpha) = \mathscr{D}_\alpha \frac{\partial^2 \phi_\alpha}{\partial x_i \partial x_i}, \tag{2.1}$$

where ϕ_α is the local concentration of species α, u_i is the Navier–Stokes velocity, and $\mathscr{D}_\alpha$ denotes the molecular diffusivity. As the turbulence is isotropic, we assume, without loss of generality, that there is zero mean flow (Hinze 1975; Lesieur 1987); thus, after a Reynolds decomposition, $u_i = u_i'$. A similar equation for ϕ_β can be written by analogy.

2.1. *Isotropic scalar*

First, we consider the example of two coherently forced isotropic scalars. Coherent forcing is done by introducing identical, stochastic source terms into the scalar equations. The scalar forcing is applied to wavenumbers less than $\sqrt{2}$, and uses an algorithm that is similar to that used for the energy (see Eswaran & Pope 1988 for details). In the absence of differential diffusion, both scalars would remain equal under the present forcing, and so the statistical separation of the two scalars is a direct measure of differential diffusion. For this case, we assume (again without loss of generality) that the mean scalar concentration is zero; thus, we have $\phi_\alpha = \phi_\alpha'$. The governing equations for each scalar can be made dimensionless by using the integral length scale of the turbulence L (for x_i), the r.m.s. fluctuating velocity u' (for u_i'), and the large eddy turnover time L/u' (for t). Characteristic scalar fluctuations then can be defined in terms of the scalar dissipation rates

$$\chi_\alpha = 2\mathscr{D}_\alpha \overline{\nabla \phi_\alpha' \cdot \nabla \phi_\alpha'}, \tag{2.2}$$

$$\chi_\beta = 2\mathscr{D}_\beta \overline{\nabla \phi_\beta' \cdot \nabla \phi_\beta'}, \tag{2.3}$$

$$\chi_{\alpha\beta} = (\mathscr{D}_\alpha + \mathscr{D}_\beta) \overline{\nabla \phi_\alpha' \cdot \nabla \phi_\beta'}, \tag{2.4}$$

yielding $(\chi_\alpha L/u')^{1/2}$ and $(\chi_\beta L/u')^{1/2}$ (for ϕ_α' and ϕ_β', respectively). The resulting dimensionless equations become

$$\frac{\partial \phi_\alpha'}{\partial t} + \frac{\partial}{\partial x_i}(u_i' \phi_\alpha') = \frac{1}{Pe_\alpha} \frac{\partial^2 \phi_\alpha'}{\partial x_i \partial x_i}, \tag{2.5}$$

$$\frac{\partial \phi_\beta'}{\partial t} + \frac{\partial}{\partial x_i}(u_i' \phi_\beta') = \frac{1}{Pe_\beta} \frac{\partial^2 \phi_\beta'}{\partial x_i \partial x_i}, \tag{2.6}$$

where Pe_α, the mass transfer Péclet number, is defined in terms of the Reynolds and Schmidt numbers ($Re_L = u'L/\nu$ and $Sc_\alpha = \nu/\mathscr{D}_\alpha$) as $Pe_\alpha = Re_L Sc_\alpha$. The definitions of Sc_β and Pe_β follow by analogy. Also note that in order to maintain a reasonable nomenclature, the same variables (e.g. x_i, t, u_i' and ϕ') have been used to represent dimensionless and dimensional quantities. Since all subsequent equations will be expressed in dimensionless form (except where noted), this practice should not cause any confusion.

The relevant correlations for isotropic scalars are

$$B^{\alpha}(\boldsymbol{x}_1, \boldsymbol{x}_2) \equiv \overline{\phi'_{\alpha}(\boldsymbol{x}_1)\phi'_{\alpha}(\boldsymbol{x}_2)}, \tag{2.7}$$

$$B^{\beta}(\boldsymbol{x}_1, \boldsymbol{x}_2) \equiv \overline{\phi'_{\beta}(\boldsymbol{x}_1)\phi'_{\beta}(\boldsymbol{x}_2)}, \tag{2.8}$$

$$B^{\alpha\beta}(\boldsymbol{x}_1, \boldsymbol{x}_2) \equiv \overline{\phi'_{\alpha}(\boldsymbol{x}_1)\phi'_{\beta}(\boldsymbol{x}_2)}. \tag{2.9}$$

From the definition of the Fourier transform,

$$B^{i}(\boldsymbol{k}, \boldsymbol{p}) \equiv \iint B^{i}(\boldsymbol{x}_1, \boldsymbol{x}_2) \exp(-\mathrm{I}(\boldsymbol{k} \cdot \boldsymbol{x}_1 + \boldsymbol{p} \cdot \boldsymbol{x}_2))\, \mathrm{d}\boldsymbol{x}_1\, \mathrm{d}\boldsymbol{x}_2, \tag{2.10}$$

and its inverse,

$$B^{i}(\boldsymbol{x}_1, \boldsymbol{x}_2) \equiv \iint B^{i}(\boldsymbol{k}, \boldsymbol{p}) \exp(+\mathrm{I}(\boldsymbol{k} \cdot \boldsymbol{x}_1 + \boldsymbol{p} \cdot \boldsymbol{x}_2))\, \hat{\mathrm{d}}\boldsymbol{k}\, \hat{\mathrm{d}}\boldsymbol{p}, \tag{2.11}$$

where $\mathrm{I} \equiv \sqrt{-1}$, i refers to α, β or $\alpha\beta$, $\hat{\mathrm{d}}\boldsymbol{k} \equiv \mathrm{d}\boldsymbol{k}/(2\pi)^3$ and $\hat{\mathrm{d}}\boldsymbol{p} \equiv \mathrm{d}\boldsymbol{p}/(2\pi)^3$, it can be shown that for an isotropic scalar spectrum

$$B^{i}(\boldsymbol{k}, \boldsymbol{p}) = 2\hat{\delta}(\boldsymbol{k} + \boldsymbol{p}) B^{i}(k), \tag{2.12}$$

where $\hat{\delta}(\boldsymbol{k}) \equiv (2\pi)^3 \delta(\boldsymbol{k})$ and $\delta(\boldsymbol{k})$ is the three-dimensional Dirac delta function. Note that the arguments for $B^{i}(\boldsymbol{k}, \boldsymbol{p})$ and $B^{i}(k)$ in (2.12) uniquely define the function and its dimensional units. $B^{i}(k)$ is related to the traditional scalar spectrum by $E^{i}_{\phi}(k) = k^2 B^{i}(k)/\pi^2$.

The governing equation for the scalar covariance spectrum is

$$\left[\frac{\partial}{\partial t} + \left(\frac{1}{Pe_{\alpha}} + \frac{1}{Pe_{\beta}}\right) k^2\right] B^{\alpha\beta}(k) = Tr^{\alpha\beta}_{B}(k) + F^{\alpha\beta}(k), \tag{2.13}$$

where $Tr^{\alpha\beta}_{B}(k)$ is the transfer spectrum that is modelled by the EDQNM theory (note 'transfer spectrum' refers to the nonlinear advective term in the equation for $B^{\alpha\beta}(k)$) and $F^{\alpha\beta}(k)$ is the low-wavenumber forcing function for the scalar energy that corresponds to the coherent source term in the scalar field equations. Equations for the two autocorrelation spectra, $B^{\alpha}(k)$ and $B^{\beta}(k)$, are obtained from (2.13) by setting β equal to α or vice versa. The EDQNM model for the transfer function is

$$Tr^{i}_{B}(k) = \int\!\!\int_{\Delta} [g(k,p,q)E(p)B^{i}(q) - g(q,p,k)E(p)B^{i}(k)]\theta(\mu^{pkq}_{M})\, \mathrm{d}p\, \mathrm{d}q, \tag{2.14}$$

where $E(k)$ is the turbulent energy spectrum and Δ refers to an integration over all p and q that form a triad with k. The geometric factor $g(k,p,q)$ is defined as

$$g(k,p,q) \equiv \frac{N^2 k}{p^3 q}, \tag{2.15}$$

where

$$N^2 = \tfrac{1}{4}((k+p+q)(k+p-q)(p+q-k)(q+k-p)). \tag{2.16}$$

The time-dependent function, $\theta(\gamma)$, is given by

$$\theta(\gamma) = \frac{1 - \mathrm{e}^{-\gamma t}}{\gamma}. \tag{2.17}$$

UC showed that the inverse time scale, μ^{pkq}_{M}, that comes out of the standard Markovianization procedure produces an unrealizable covariance spectrum. The mathematical argument in UC, based on a Langevin equation analysis, rigorously proved that the

inverse time scale must be independent of the scalar diffusivities to satisfy the Cauchy–Schwartz condition and conservation simultaneously. A physical explanation of this result is that scalar transfer, a convective process, should not depend explicitly upon the scalar molecular properties, as this allows two spatially identical scalars to transfer at different rates owing to differences in their molecular diffusivities – an impossible result. The origin of the error appears to be the Markovianization step, where an artificial dependence on the molecular diffusivity arises. This presents no realizability problem for a single scalar; however, for multiple scalars, the explicit dependence of the transfer functions on the molecular diffusivities causes a violation of the Cauchy–Schwartz condition for the scalar covariance spectrum. UC proposed the following modified inverse time scale,

$$\mu_M^{pkq} \equiv c_{1M}\mu^p + c_{2M}\,(\mu^k + \mu^q) + \frac{1}{Re_L}(p^2 + k^2 + q^2), \tag{2.18}$$

where μ^k is calculated in the manner suggested by Pouquet *et al.* (1975)

$$\mu^k = \sqrt{\int_0^k \tilde{k}^2 E(\tilde{k})\,\mathrm{d}\tilde{k}}. \tag{2.19}$$

Notice that the dependence of μ_M^{pkq} on the scalar diffusivity (Péclet number) is replaced by the kinematic viscosity (Reynolds number). This modified inverse time scale yields realizable results under all conditions.

There are two unknown constants in the model, c_{1M} and c_{2M}. Following the analysis of Herring *et al.* (1982), the coefficients c_{1M} and c_{2M} are assigned values of 0.36.

2.2. *Uniform mean scalar gradient*

For the case of the uniform mean gradient, the analysis is complicated in two ways. First, the reduction in symmetry implies that all correlations involving either scalar are axisymmetric, and therefore are functions of the wavenumber (as before) and the angle between the wavevector $\boldsymbol{k}$ and the direction of the mean gradient, here taken to be in the x_3-direction. We define the cosine of this angle as μ. Following Herring (1974), we express this implicit dependence on μ explicitly in terms of an infinite Legendre polynomial series. Secondly, the mean gradient creates a turbulent scalar flux aligned along the direction of the mean gradient. This introduces two coupled scalar–velocity correlations that must be solved for simultaneously.

The non-dimensional equations for each scalar fluctuation become

$$\frac{\partial \phi'_\alpha}{\partial t} + \frac{\partial}{\partial x_i}(u'_i\phi'_\alpha) + u'_3 = \frac{1}{Pe_\alpha}\frac{\partial^2 \phi'_\alpha}{\partial x_i \partial x_i}, \tag{2.20}$$

$$\frac{\partial \phi'_\beta}{\partial t} + \frac{\partial}{\partial x_i}(u'_i\phi'_\beta) + u'_3 = \frac{1}{Pe_\beta}\frac{\partial^2 \phi'_\beta}{\partial x_i \partial x_i}, \tag{2.21}$$

where we now non-dimensionalize the scalar fluctuations ϕ'_α and ϕ'_β by the characteristic scalar fluctuation $\Gamma_\alpha L$ and $\Gamma_\beta L$, respectively, where Γ_α and Γ_β are the magnitudes of the mean gradient of each species.

In addition to the two-point correlations identified in (2.7)–(2.9), the autocorrelation and covariance spectra in the presence of a uniform mean gradient will further depend upon the following scalar–velocity correlations

$$Q_i^\alpha(\boldsymbol{x}_1, \boldsymbol{x}_2) \equiv \overline{u'_i(\boldsymbol{x}_1)\phi'_\alpha(\boldsymbol{x}_2)}, \tag{2.22}$$

$$Q_i^\beta(\boldsymbol{x}_1, \boldsymbol{x}_2) \equiv \overline{u'_i(\boldsymbol{x}_1)\phi'_\beta(\boldsymbol{x}_2)}. \tag{2.23}$$

For the mirror-symmetric (i.e. non-helical) isotropic velocity field considered in this study, the Fourier transform of the scalar–velocity covariance spectrum can be written as follows (Batchelor 1946; Chandrasekhar 1950)

$$Q_i^{\alpha}(\boldsymbol{k},\boldsymbol{p}) = \hat{\delta}(\boldsymbol{k}+\boldsymbol{p})P_{i3}(\boldsymbol{k})Q^{\alpha}(k,\mu), \tag{2.24}$$

where $P_{ij}(\boldsymbol{k}) = \delta_{ij} - k_i k_j/k^2$ is the projection operator and $Q^{\alpha}(k,\mu)$ is a real function of the wavenumber k and angle μ. The governing equation for $Q^{\alpha}(k,\mu)$ is (Herr *et al.* 1996)

$$\begin{aligned}\left[\frac{\partial}{\partial t} + \left(\frac{1}{Re_L} + \frac{1}{Pe_{\alpha}}\right)k^2\right](1-\mu^2)Q^{\alpha}(k,\mu) \\ = \underbrace{-k_j P_{i3}(\boldsymbol{k}) \iint T_{ij}^{\alpha}(\boldsymbol{k},\boldsymbol{p},\boldsymbol{q})\,\hat{\mathrm{d}}\boldsymbol{p}\,\hat{\mathrm{d}}\boldsymbol{q} - \tfrac{1}{2}P_{3ij}(\boldsymbol{k}) \iint T_{ij}^{\alpha}(\boldsymbol{q},\boldsymbol{p},\boldsymbol{k})\,\hat{\mathrm{d}}\boldsymbol{p}\,\hat{\mathrm{d}}\boldsymbol{q}}_{\text{inertial transfer}} \\ \underbrace{-(1-\mu^2)R(k)}_{\text{source}},\end{aligned} \tag{2.25}$$

in which $P_{ijm}(\boldsymbol{k}) = k_m P_{ij}(\boldsymbol{k}) + k_j P_{im}(\boldsymbol{k})$, $R(k) = 2\pi^2 E(k)/k^2$ and $T_{ij}^{\alpha}(\boldsymbol{k},\boldsymbol{p},\boldsymbol{q})$ is given by

$$T_{ij}^{\alpha}(\boldsymbol{k},\boldsymbol{p},\boldsymbol{q}) = \left[\mathscr{T}_{ij}^{\alpha}(\boldsymbol{k},\boldsymbol{p},\boldsymbol{q}) - \frac{\mathscr{R}_{ij3}(\boldsymbol{k},\boldsymbol{p},\boldsymbol{q})}{\mu_R^{kpq}}\right]\theta(\mu_T^{kpq}). \tag{2.26}$$

The equation for $Q^{\beta}(k,\mu)$ follows by analogy. Expressions for $\mathscr{T}_{ij}^{\alpha}(\boldsymbol{k},\boldsymbol{p},\boldsymbol{q})$ and $\mathscr{R}_{ij3}(\boldsymbol{k},\boldsymbol{p},\boldsymbol{q})$ are given in table 1. The coefficient μ_R^{kpq} retains its classical definition

$$\mu_R^{kpq} = c_R(\mu^k + \mu^p + \mu^q) + \frac{1}{Re_L}(k^2+p^2+q^2), \tag{2.27}$$

whereas the modified coefficient μ_T^{kpq} suggested by UC is

$$\mu_T^{kpq} = c_{1T}(\mu^k + \mu^p) + c_{2T}\mu^q + \frac{1}{Re_L}(k^2+p^2+q^2), \tag{2.28}$$

in which the explicit dependence on the Péclet number has again been removed.

The anisotropic scalar covariance spectrum, $B^{\alpha\beta}(k,\mu)$, is governed by

$$\begin{aligned}\left[\frac{\partial}{\partial t} + \left(\frac{1}{Pe_{\alpha}} + \frac{1}{Pe_{\beta}}\right)k^2\right]B^{\alpha\beta}(k,\mu) = \underbrace{-k_i \iint \tfrac{1}{2}[M_i^{\alpha\beta}(\boldsymbol{p},\boldsymbol{k},\boldsymbol{q}) + M_i^{\beta\alpha}(\boldsymbol{p},\boldsymbol{k},\boldsymbol{q})]\,\hat{\mathrm{d}}\boldsymbol{p}\,\hat{\mathrm{d}}\boldsymbol{q}}_{\text{inertial transfer}} \\ \underbrace{-\tfrac{1}{2}(1-\mu^2)[Q^{\alpha}(k,\mu) + Q^{\beta}(k,\mu)]}_{\text{source}},\end{aligned} \tag{2.29}$$

where

$$\begin{aligned}M_i^{\alpha\beta}(\boldsymbol{k},\boldsymbol{p},\boldsymbol{q}) = &\left[\frac{\mathscr{R}_{i33}(\boldsymbol{k},\boldsymbol{p},\boldsymbol{q})}{\mu_R^{kpq}} - \mathscr{T}_{i3}^{\beta}(\boldsymbol{k},\boldsymbol{p},\boldsymbol{q})\right]\xi(\mu_T^{kpq},\mu_M^{kpq}) \\ &+ \left[\frac{\mathscr{R}_{i33}(\boldsymbol{k},\boldsymbol{q},\boldsymbol{p})}{\mu_R^{kqp}} - \mathscr{T}_{i3}^{\alpha}(\boldsymbol{k},\boldsymbol{q},\boldsymbol{p})\right]\xi(\mu_T^{kqp},\mu_M^{kpq}) \\ &+ \mathscr{M}_i^{\alpha\beta}(\boldsymbol{k},\boldsymbol{p},\boldsymbol{q})\theta(\mu_M^{kpq}),\end{aligned} \tag{2.30}$$

$$\mathscr{R}_{ij3}(\boldsymbol{k},\boldsymbol{p},\boldsymbol{q}) \quad \{-P_{iab}(\boldsymbol{k})P_{ja}(\boldsymbol{p})P_{b3}(\boldsymbol{q})R(p)R(q) - P_{jab}(\boldsymbol{p})P_{ia}(\boldsymbol{k})P_{b3}(\boldsymbol{q})R(k)R(q) - P_{3ab}(\boldsymbol{q})P_{ia}(\boldsymbol{k})P_{jb}(\boldsymbol{p})R(k)R(p)\}\,\hat{\delta}(\boldsymbol{k}+\boldsymbol{p}+\boldsymbol{q})$$

$$\mathscr{T}^{\alpha}_{ij}(\boldsymbol{k},\boldsymbol{p},\boldsymbol{q}) \quad \{-P_{jab}(\boldsymbol{p})P_{ia}(\boldsymbol{k})P_{b3}(\boldsymbol{q})Q^{\alpha}(q,\mu'')R(k) - P_{iab}(\boldsymbol{k})P_{aj}(\boldsymbol{p})P_{b3}(\boldsymbol{q})Q^{\alpha}(q,\mu'')R(p) - q_nP_{in}(\boldsymbol{k})P_{j3}(\boldsymbol{p})Q^{\alpha}(p,\mu')R(k) - q_nP_{jn}(\boldsymbol{p})P_{i3}(\boldsymbol{k})Q^{\alpha}(k,\mu)R(p)\}\,\hat{\delta}(\boldsymbol{k}+\boldsymbol{p}+\boldsymbol{q})$$

$$\mathscr{T}^{\beta}_{ij}(\boldsymbol{k},\boldsymbol{p},\boldsymbol{q}) \quad \{-P_{jab}(\boldsymbol{p})P_{ia}(\boldsymbol{k})P_{b3}(\boldsymbol{q})Q^{\beta}(q,\mu'')R(k) - P_{iab}(\boldsymbol{k})P_{aj}(\boldsymbol{p})P_{b3}(\boldsymbol{q})Q^{\beta}(q,\mu'')R(p) - q_nP_{in}(\boldsymbol{k})P_{j3}(\boldsymbol{p})Q^{\beta}(p,\mu')R(k) - q_nP_{jn}(\boldsymbol{p})P_{i3}(\boldsymbol{k})Q^{\beta}(k,\mu)R(p)\}\,\hat{\delta}(\boldsymbol{k}+\boldsymbol{p}+\boldsymbol{q})$$

$$\mathscr{M}^{\alpha\beta}_{i}(\boldsymbol{k},\boldsymbol{p},\boldsymbol{q}) \quad \{-2p_jP_{ij}(\boldsymbol{k})R(k)B^{\alpha\beta}(q,\mu'') - 2q_jP_{ij}(\boldsymbol{k})R(k)B^{\alpha\beta}(p,\mu') - p_jP_{i3}(\boldsymbol{k})P_{j3}(\boldsymbol{q})Q^{\alpha}(k,\mu)Q^{\beta}(q,\mu'') - q_jP_{i3}(\boldsymbol{k})P_{j3}(\boldsymbol{p})Q^{\beta}(k,\mu)Q^{\alpha}(p,\mu') - P_{iab}(\boldsymbol{k})P_{a3}(\boldsymbol{p})P_{b3}(\boldsymbol{q})Q^{\alpha}(p,\mu')Q^{\beta}(q,\mu'')\}\,\hat{\delta}(\boldsymbol{k}+\boldsymbol{p}+\boldsymbol{q})$$

TABLE 1. Explicit representation of triple correlations.

$\mathscr{M}^{\alpha\beta}_{i}(\boldsymbol{k},\boldsymbol{p},\boldsymbol{q})$ is given in table 1, μ^{kpq}_{M} is defined in (2.18), and the new time-dependent function, $\xi(\gamma,\delta)$, is given by

$$\xi(\gamma,\delta) = \begin{cases} \dfrac{1}{\gamma}\left[\dfrac{1-\mathrm{e}^{-\delta t}}{\delta} + \dfrac{\mathrm{e}^{-\gamma t}-\mathrm{e}^{-\delta t}}{\gamma-\delta}\right], & \gamma \neq \delta, \\ \dfrac{1}{\gamma}\left[\dfrac{1-\mathrm{e}^{-\gamma t}}{\gamma} - t\mathrm{e}^{-\gamma t}\right], & \gamma = \delta. \end{cases} \tag{2.31}$$

Equations for $B^{\alpha}(k,\mu)$ and $B^{\beta}(k,\mu)$ follow by analogy.

Application of the Legendre expansion for the μ dependence (Herring 1974) yields an infinite series; however, Herr *et al.* (1996) showed that for the conditions of this calculation, $Q^{j}(k,\mu)$ is isotropic (i.e. $Q^{j}(k,\mu) = Q^{j}(k)$, where j is α or β). This reduction assumes the scalar fluctuations are initially zero and subsequently arise soley from the presence of the uniform mean gradient. Under this circumstance, the μ dependence in the $Q^{j}(k,\mu)$ equation cancels out because each of the transfer and source terms has the same $(1-\mu^2)$ dependence. Likewise, the Legendre expansion for the scalar–scalar spectra are limited to the first two terms, i.e. $B^{i}(k,\mu) = B^{i}_{0}(k) + B^{i}_{2}(k)(3\mu^2-1)/2$ (where i is α, β or $\alpha\beta$); higher-order terms in the series are identically zero. By taking advantage of the orthogonal properties of Legendre polynomials, it is possible to derive separate equations for $B^{i}_{0}(k)$ and $B^{i}_{2}(k)$ (see Herr *et al.* 1996 for details).

For consistency with the earlier work, the coefficients are assigned the following values: $c_R = c_{1M} = c_{2M} = 0.36$. As discussed extensively in Herr *et al.* (1996), the constants that arise in the Q-equation, c_{1T} and c_{2T}, are not constrained by a conservation principle. Instead, they are determined by fitting to experimental or DNS data. Comparisons with DNS, presented in § 3.2, suggest a better overall fit is obtained using $c_{1T} = 0$ and $c_{2T} = 0.83$.

2.3. *Statistical quantities of interest*

The equations for $B^{\alpha}(k)$, $B^{\beta}(k)$ and $B^{\alpha\beta}(k)$ for the forced isotropic scalar and $B^{\alpha}_{0}(k)$, $B^{\beta}_{0}(k)$, $B^{\alpha\beta}_{0}(k)$, $B^{\alpha}_{2}(k)$, $B^{\beta}_{2}(k)$, $B^{\alpha\beta}_{2}(k)$, $Q^{\alpha}(k)$ and $Q^{\beta}(k)$ for the case of the mean gradient were integrated numerically on a uniform grid with either 64 or 256 wavenumbers (corresponding respectively to a direct numerical simulation with 128^3 or 512^3 points

in the physical domain). Details of the numerical method can be found in Herr *et al.* (1996).

We focus mainly on single-point and spectral properties of the scalar fields. The scalar spectrum is defined as

$$E_\phi^i(k) \equiv \frac{1}{(2\pi)^3} \int \int B^i(\boldsymbol{k}, \boldsymbol{p})\, \hat{\mathrm{d}}\boldsymbol{p}\, k^2\, \mathrm{d}\Omega_k = \frac{k^2 B_0^i(k)}{\pi^2}, \tag{2.32}$$

where $\mathrm{d}\Omega_k$ is the solid angle for wavevector $\boldsymbol{k}$ and the subscript 0 on the far right-hand side is suppressed for the isotropic scalar. The scalar–velocity spectrum that arises in the case of the uniform mean gradient is defined as

$$E_Q^j(k) \equiv \frac{1}{(2\pi)^3} \int \int Q_3^j(\boldsymbol{k}, \boldsymbol{p})\, \hat{\mathrm{d}}\boldsymbol{p}\, k^2\, \mathrm{d}\Omega_k = \frac{Q^j(k) k^2}{3\pi^2}. \tag{2.33}$$

We can calculate the scalar fluctuation intensity by

$$\Phi_{\mathrm{rms}}^i = \left(\int_0^{k_{\max}} E_\phi^i(k)\, \mathrm{d}k \right)^{1/2}, \tag{2.34}$$

and the turbulent scalar flux in the direction of the mean gradient by

$$\overline{u_3' \phi_\alpha'} = \int_0^{k_{\max}} E_Q^\alpha(k)\, \mathrm{d}k. \tag{2.35}$$

Following Yeung (1996), we define a correlation coefficient in the following manner

$$\tilde{\rho} \equiv \frac{\left(\Phi_{\mathrm{rms}}^{\alpha\beta}\right)^2}{\Phi_{\mathrm{rms}}^\alpha \Phi_{\mathrm{rms}}^\beta}. \tag{2.36}$$

The spectral equivalent is the coherency spectrum (normalized spectral scalar covariance spectrum), which is computed according to

$$\rho(k) = \frac{E_\phi^{\alpha\beta}(k)}{\sqrt{E_\phi^\alpha(k) E_\phi^\beta(k)}}. \tag{2.37}$$

3. Comparison with DNS

In this section, we present comparisons of the modified EDQNM model with DNS for both the isotropically forced scalar and the scalar with a uniform mean gradient. The simulations were similar to earlier ones performed in our group (e.g. see Herr *et al.* 1996), hence, we will present only an overview of the numerical method and refer the interested reader to the original source for details. The Navier–Stokes and scalar transport equations were integrated in three spatial dimensions and time using a pseudospectral algorithm on a 128^3 grid. The turbulent energy was made stationary by forcing wavenumbers less than $\sqrt{2}$ using an algorithm similar to Eswaran & Pope (1988). The initial velocity field and forcing were fixed for all of the simulations. We calculated an energy spectrum by averaging the instantaneous spectrum over 30 eddy turnover times at one eddy turnover time intervals. This energy spectrum is shown in figure 1 and the pertinent parameters are summarized in table 2.

Rather than solve for the energy spectrum using the EDQNM model, we substitute the average energy spectrum obtained from the DNS, thereby eliminating a possible source of error. In addition to the turbulence parameters, the Schmidt number for each scalar field must be defined. Three combinations of Schmidt numbers have been

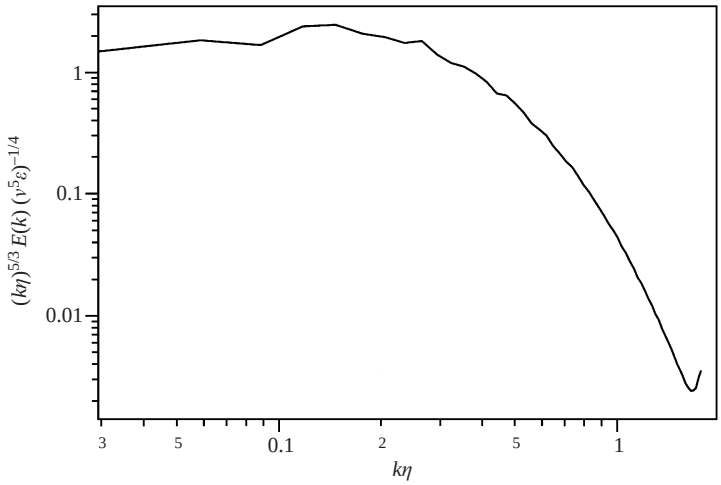

FIGURE 1. Average turbulent energy spectrum shown in Kolmogorov-compensated coordinates, in which ϵ is the dissipation rate and $\eta \equiv (\nu^3/\epsilon)^{1/4}$ is the Kolmogorov length scale. The spectrum was obtained by averaging 30 instantaneous spectra at one eddy turnover time intervals.

Parameter	Definition	Value
u'	Turbulence intensity	1.00
ϵ	Dissipation rate	0.33
ν	Kinematic viscosity	6.3×10^{-3}
L	Integral length scale	1.51
λ	Taylor microscale	0.53
η	Kolmogorov length scale	0.03
T_e	Eddy turnover time	1.51
Re_L	Reynolds number (integral scale)	239
Re_λ	Reynolds number (Taylor microscale)	85
$k_{\max}\eta$	Resolution criterion	1.78

TABLE 2. Turbulence parameters associated with the energy spectrum in arbitrary units (except for the last three quantities which are dimensionless).

considered and they are designated as case (i): $Sc_\alpha = 1$ and $Sc_\beta = \frac{1}{4}$; case (ii): $Sc_\alpha = 1$ and $Sc_\beta = \frac{1}{16}$; and case (iii): $Sc_\alpha = \frac{1}{4}$ and $Sc_\beta = \frac{1}{16}$.

3.1. *Isotropic scalar*

Recall that the isotropic scalar field arises from a coherent source term in the scalar equations. Even though the source for each scalar is identical, the forcing delivered to the scalar spectra, $F^\alpha(k)$, $F^\beta(k)$ and $F^{\alpha\beta}(k)$, are not necessarily the same owing to differences in the correlation of the source with each scalar. We therefore must set $F^\alpha(k)$, $F^\beta(k)$ and $F^{\alpha\beta}(k)$ independently in the model. We are interested mainly in comparing the steady state EDQNM predictions with stationary results from the DNS. At steady state the dimensional forcing functions satisfy the following constraints

$$\frac{1}{\pi^2}\int_0^{k_{\max}} k^2 F^\alpha(k) = \chi_\alpha,$$

Case	χ_α	χ_β	$\chi_{\alpha\beta}$
(i)	0.3627	0.3544	0.3585
(ii)	0.3627	0.3201	0.3414
(iii)	0.3544	0.3201	0.3372

TABLE 3. Dissipation rates for isotropic scalar DNS for $Sc_\alpha = 1$ and $Sc_\beta = \frac{1}{4}$ (case (i)), $Sc_\alpha = 1$ and $Sc_\beta = \frac{1}{16}$ (case (ii)), and $Sc_\alpha = \frac{1}{4}$ and $Sc_\beta = \frac{1}{16}$ (case (iii)).

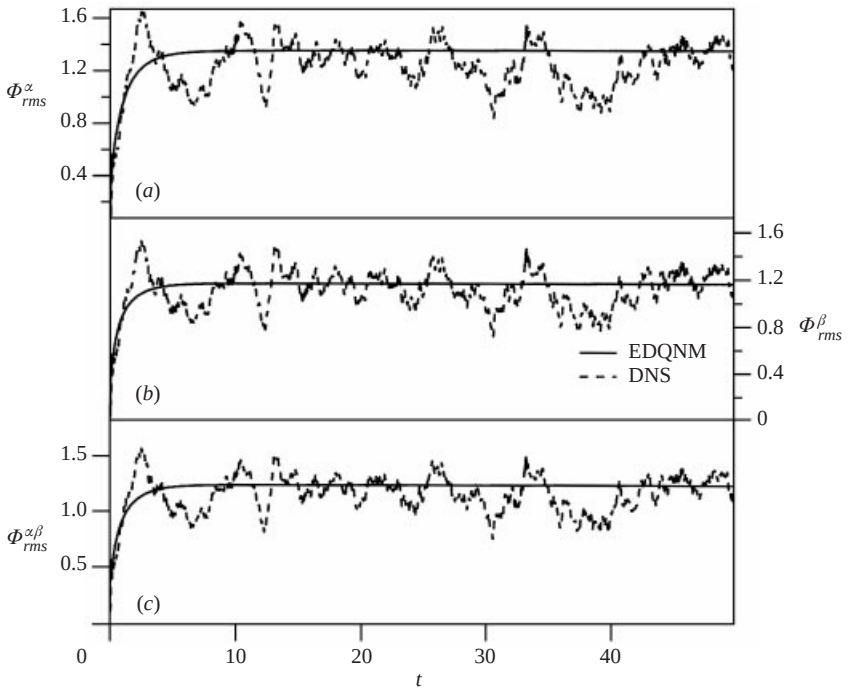

FIGURE 2. Scalar intensity (*a*) $\Phi^{\alpha}_{\rm rms}$, (*b*) $\Phi^{\beta}_{\rm rms}$ and (*c*) $\Phi^{\alpha\beta}_{\rm rms}$ (see (2.34) for definitions) as a function of dimensionless time (made dimensionless with the large eddy turnover time) for case (i) of the forced isotropic scalar study.

$$\frac{1}{\pi^2}\int_0^{k_{\max}} k^2 F^\beta(k) = \chi_\beta,$$

where by definition

$$F^{\alpha\beta}(k) = \tfrac{1}{2}(F^\alpha(k) + F^\beta(k)).$$

The mean scalar dissipation rates from the DNS are summarized in table 3. To be consistent with the DNS, only the first two wavenumbers of $F^\alpha(k)$ and $F^\beta(k)$ are non-zero. These constraints leave only one additional degree of freedom for each of the forcing parameters that was used to match the integral length scale of each autocorrelation spectrum from the DNS.

Figures 2 and 3 show a comparison of the DNS and EDQNM scalar intensities for cases (i) and (ii), respectively. The overall agreement between the simulations and the model is very good. Similar agreement is found for the correlation coefficient shown in figure 4. There is some disagreement at short times, which is most probably

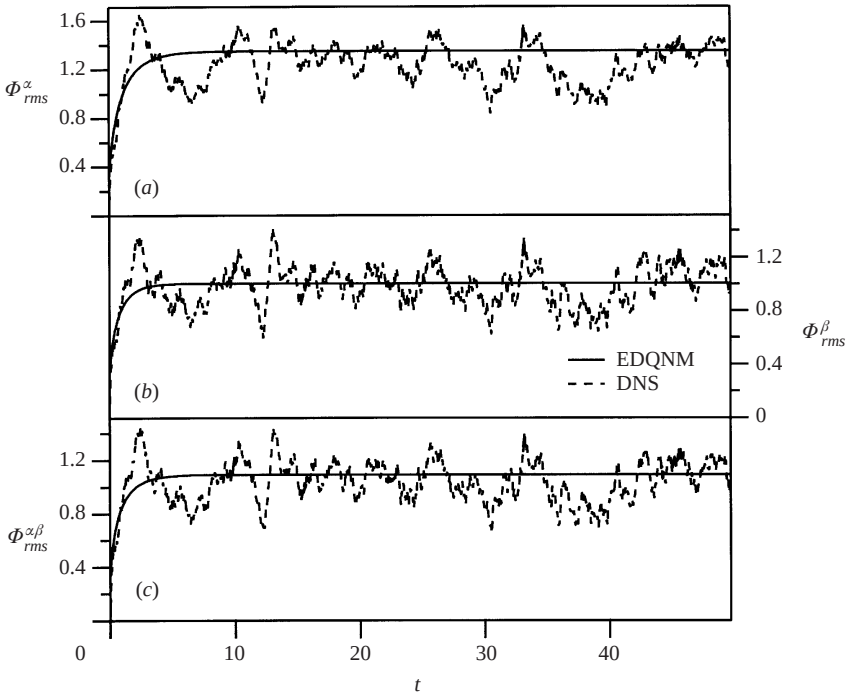

FIGURE 3. Scalar intensity (*a*) $\Phi^{\alpha}_{\rm rms}$, (*b*) $\Phi^{\beta}_{\rm rms}$ and (*c*) $\Phi^{\alpha\beta}_{\rm rms}$ as a function of dimensionless time for case (ii) of the forced isotropic scalar study.

Case	DNS	EDQNM	% Error
$\Phi^{\alpha}_{\rm rms}(Sc = 1)$	1.2436	1.3488	8.2
$\Phi^{\alpha}_{\rm rms}(Sc = \frac{1}{4})$	1.1161	1.1638	4.2
$\Phi^{\alpha}_{\rm rms}(Sc = \frac{1}{16})$	0.9836	1.0058	2.2
$\Phi^{\alpha\beta}_{\rm rms}$ (case (i))	1.1583	1.2333	6.4
$\Phi^{\alpha\beta}_{\rm rms}$ (case (ii))	1.0384	1.0915	5.1
$\tilde{\rho}$ (case (i))	0.9668	0.9689	0.2
$\tilde{\rho}$ (case (ii))	0.8809	0.8783	−0.2

TABLE 4. Comparison of averaged statistics from DNS with EDQNM model predictions for all of the single-point quantities.

due to the mismatch in the scalar forcing over this period. A summary of all of the single-point statistics from the model and DNS is given in table 4. We see that the maximum error for all of the cases is 8.2%, and this occurs at $Sc = 1$, where the modifications to the EDQNM model vanish. We therefore conclude that the modified EDQNM model continues to capture single-point statistics very well.

The autocorrelation and scalar covariance correlation spectra for cases (i) and (ii) are shown in figures 5 and 6. The DNS scalar spectra were obtained by averaging 30 instantaneous spectra separated by an eddy turnover time. Overall, the agreement is very good, although there are some discrepancies at higher wavenumbers. At the highest Schmidt number ($Sc = 1$), the EDQNM model for the autocorrelation spectrum underpredicts the DNS at high wavenumbers (see the top graph in figure 5),

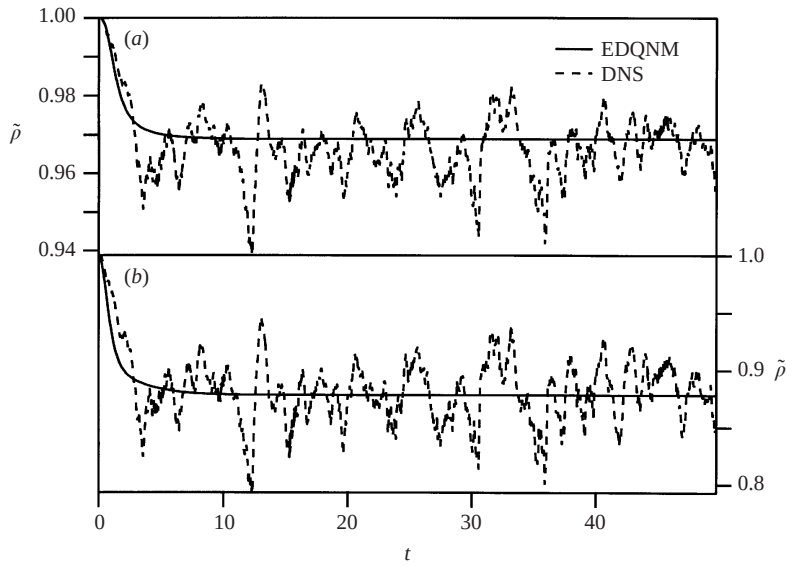

FIGURE 4. Correlation coefficient (see (2.36) for definition) for the forced isotropic scalar study as a function of time. (*a*) Case (i) and (*b*) case (ii).

whereas at the lowest Schmidt number ($Sc = \frac{1}{16}$) the opposite is true (see figure 6(*b*)). Not surprisingly, the agreement at the intermediate Schmidt number ($Sc = \frac{1}{4}$) is the best (see figure 5(*b*)). The scalar covariance spectra consistently lie in between the two autocorrelation spectra, and so their agreement with the DNS depends on the relative agreement of the autocorrelation spectra, i.e. there is excellent agreement for case (ii), where the autocorrelation spectra bracket the DNS, and somewhat lesser agreement for case (i) where the DNS is consistently above the model.

Figure 7 shows the coherency spectrum defined in (2.37). Notice here there is a more pronounced discrepancy between the EDQNM model and the DNS. Because $\rho(k)$ involves a ratio of spectra, it is a particularly sensitive measure of the performance of the model. In both cases, the DNS decays more rapidly than the model at small k, but crosses over at higher k. It is difficult to identify the origin of this discrepancy since it could involve errors in either the autocorrelation or covariance spectrum (or both). It is still encouraging that the agreement at low wavenumbers, where most of the scalar energy is located, is reasonably good, despite the fact that there are no adjustable constants in the model. It is especially encouraging that the fidelity of the model is not compromised at low Schmidt numbers, where the changes proposed by UC are greatest.

As a final test of the model, we consider the more traditional problem of a freely decaying isotropic scalar. Decaying systems introduce several challenges. First, the results are more sensitive to the initial conditions, often for all time, so care must be taken to match the initital conditions of the model and DNS accurately. Secondly, because the DNS is not stationary, we are no longer able to use time averages; instead, we perform ensemble averages over six independent realizations to reduce the statistical error. Finally, as noted by Herring *et al.* (1982), the long-time behaviour of decaying scalars is sensitive to the low wavenumber end of the spectrum. To improve the resolution of the EDQNM model at low wavenumbers, we substitute a logarithmic grid, similar to the one used in earlier EDQNM studies (Pouquet *et al.*

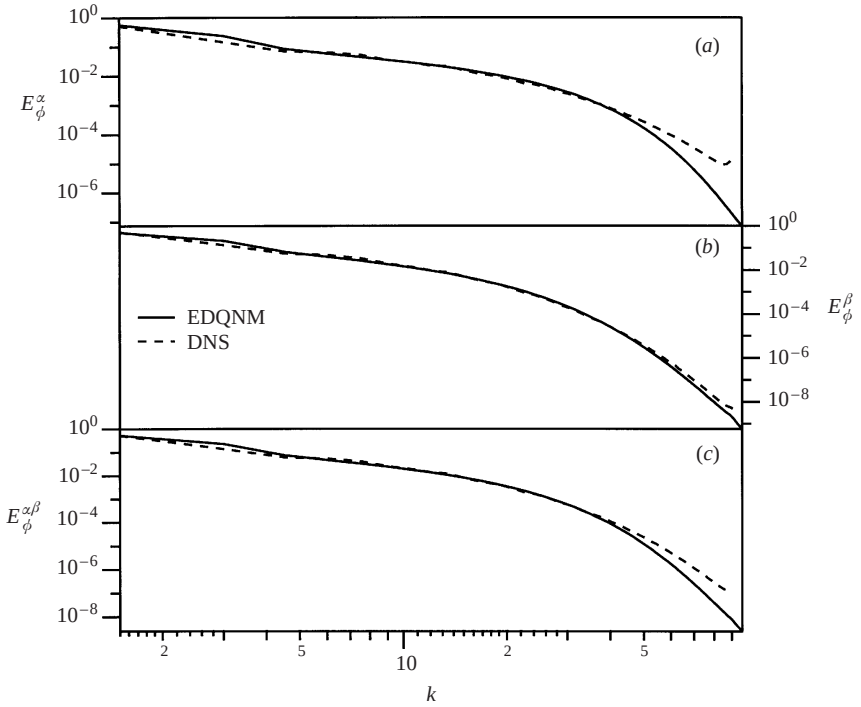

FIGURE 5. Isotropic scalar spectra for case (i). (*a*) Autocorrelation spectra for $Sc = 1$, (*b*) $Sc = \frac{1}{4}$ and (*c*) the scalar covariance spectrum. Note that the wavenumber is made dimensionless by the integral length scale.

1975; André & Lesieur 1977; Lesieur & Schertzer 1978; Herring *et al.* 1982). In this coordinate system, node points are spaced in equal increments of $\ln k$. This has the effect of increasing the density of points at small wavenumbers, which improves the accuracy of numerical evaluation of the model at long times. (Note that a comparison of EDQNM calculations using the linear and logarithmic grids for forced scalars or scalars with uniform mean gradients shows little sensitivity to the grid.)

We chose to investigate a close analogue of the decaying studies by Yeung & Pope (1993). Using the same forced energy spectrum as described above, we coherently forced two scalars with different diffusivities (case (ii): $Sc_{\alpha} = 1$ and $Sc_{\beta} = \frac{1}{16}$) for twelve eddy turnover times, and then turned the forcing off to watch the subsequent decay. The initial condition for the decay calculation was therefore the steady-state correlations we just presented. The DNS was repeated six times using the same velocity field but changing the random forcing of the scalar.

Figure 8 shows a comparison of $\tilde{\rho}(t)$ from the DNS (dashed line) with two different EDQNM calculations. The first EDQNM calculation (solid line) used 250 logarithmic grid points spread over the wavenumber range $1.51 \leqslant k \leqslant 148$. The energy spectrum was approximated by the Pao spectrum with parameters chosen to match the DNS (i.e. $u' = 0.99$, $\epsilon = 0.33$ and $Re_{\lambda} = 85$). Notice the very good agreement between this model and the DNS. The second EDQNM calculation (dotted line) used 400 logarithmic grid points spread over a much broader range of wavenumbers, $0.0025 \leqslant k \leqslant 403$. The energy spectrum was approximated by the more complete spectrum given in Pope (2000), in which the power law at low wavenumbers was assumed to be k^2. The resulting $\tilde{\rho}(t)$ is in reasonably close agreement with the DNS for the first 3–4 eddy

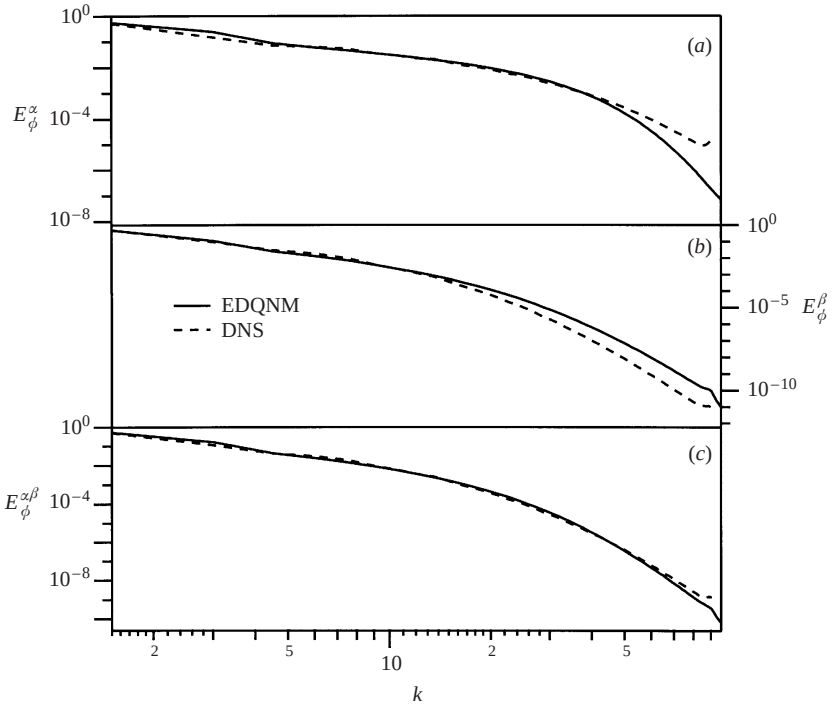

FIGURE 6. Isotropic scalar spectra for case (ii). (*a*) Autocorrelation spectra for $Sc = 1$, (*b*) $Sc = \frac{1}{16}$ and (*c*) the scalar covariance correlation spectrum.

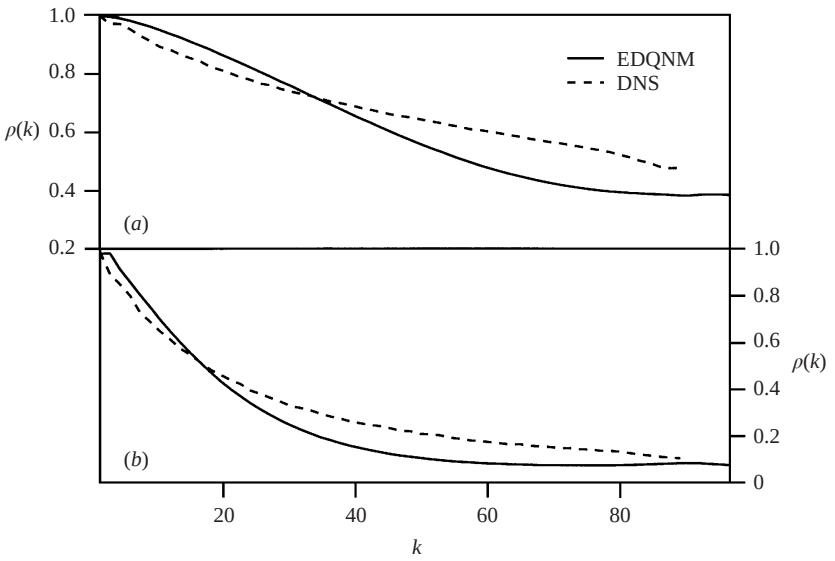

FIGURE 7. Coherency spectrum $\rho(k)$ for the forced isotropic scalar study, (*a*) case (i), (*b*) case (ii).

turnover times following the cessation of scalar forcing, but subsequently reaches a minimum and then approaches unity at long times. The qualitative difference in the behaviour of the second EDQNM calculation is due exclusively to the increase in resolution at low wavenumbers. In the latter calculation, as the scalar decays, the

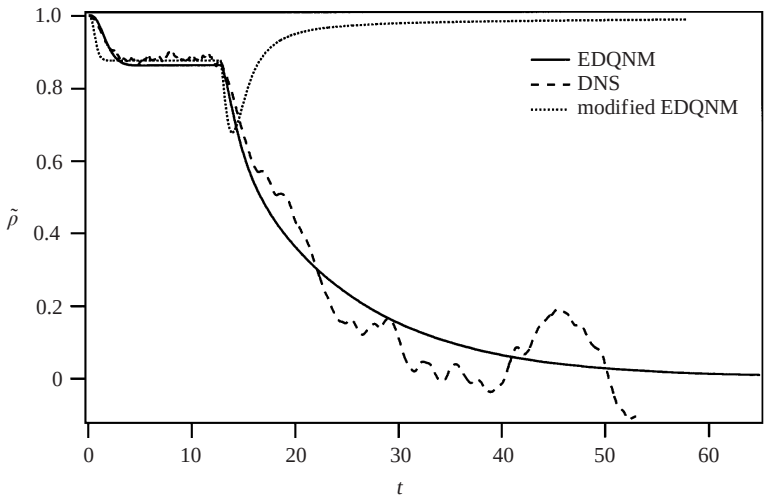

FIGURE 8. Correlation coefficient versus time for two decaying isotropic scalars with Schmidt numbers of 1 and $\frac{1}{16}$, respectively. Both scalars were coherently forced for 12 eddy turnover times, and then the forcing was abruptly turned off for the remainder of the calculation. Results from DNS (dashed line) are shown with two EDQNM calculations that are based on a logarithmic grid that spans the range $1.51 \leqslant k \leqslant 148$ (solid line) and $0.0025 \leqslant k \leqslant 403$ (dotted line).

location of the peak of the spectrum moves continuously to smaller wavenumber (i.e. larger scales). Eventually, when the peak reaches a scale that is sufficiently insensitive to differential diffusion, the scalars no longer decorrelate faster than their rate of decay. Consequently, the scalars appear to recorrelate at long times (in fact, they never decorrelated). This behaviour is not observed in the DNS because of the finite size of the box (or more precisely, the limited range of scale that can be simulated). We show this result to highlight the sensitivity of the qualitative behaviour of $\tilde{\rho}(t)$ at long times to the low wavenumber end of the spectrum. The mathematical origin of this sensitivity is most probably connected to the lack of true self-similarity over all wavenumbers, as discussed at length by Clark & Zemach (1998).

3.2. *Mean gradient*

The case of the uniform mean gradient is a more stringent test of the EDQNM model since the model now includes scalar–velocity correlations in addition to the scalar–scalar correlations and the source terms are no longer an input from the DNS, but are predicted by the model. Figures 9 and 10 compare the EDQNM and DNS values for $\Phi^{\alpha}_{\mathrm{rms}}$, $\Phi^{\beta}_{\mathrm{rms}}$ and $\Phi^{\alpha\beta}_{\mathrm{rms}}$ for cases (i) and (ii), respectively. Figure 11 shows the equivalent comparison of $\tilde{\rho}$. In general, the agreement is again excellent. Notice now the agreement at short times is even better than was found for the isotropic scalar. This is most probably due to the improvement in the representation of the source terms in the model. Figure 12 shows a comparison of the single-point turbulent flux (see (2.35) for the definition). The agreement is also very good for all three Schmidt numbers. Table 5 shows a summary of all of the single-point statistics from the mean gradient study. The maximum error for all cases is 5%.

The comparison of the scalar–scalar and scalar–velocity spectra for cases (i) and (ii) is presented in figures 13–15. Once again, the model captures the behaviour very well. Indeed, figures 13 and 14 look very similar to the equivalent isotropic spectra (see figures 5 and 6) despite the much more complex transfer that arises with the

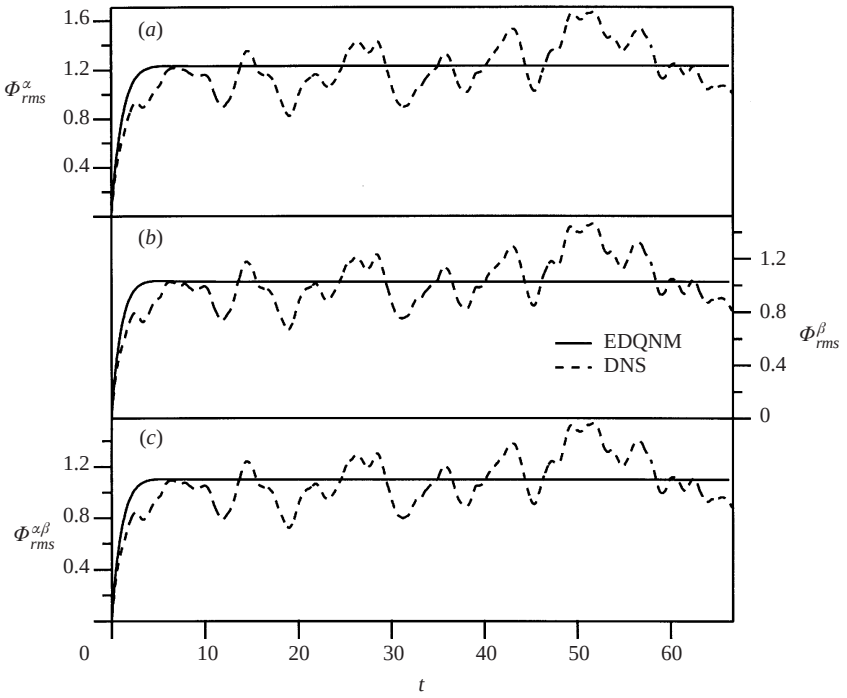

FIGURE 9. Scalar intensity (*a*) $\Phi^{\alpha}_{\rm rms}$, (*b*) $\Phi^{\beta}_{\rm rms}$ and (*c*) $\Phi^{\alpha\beta}_{\rm rms}$ as a function of dimensionless time for case (i) of the mean gradient study.

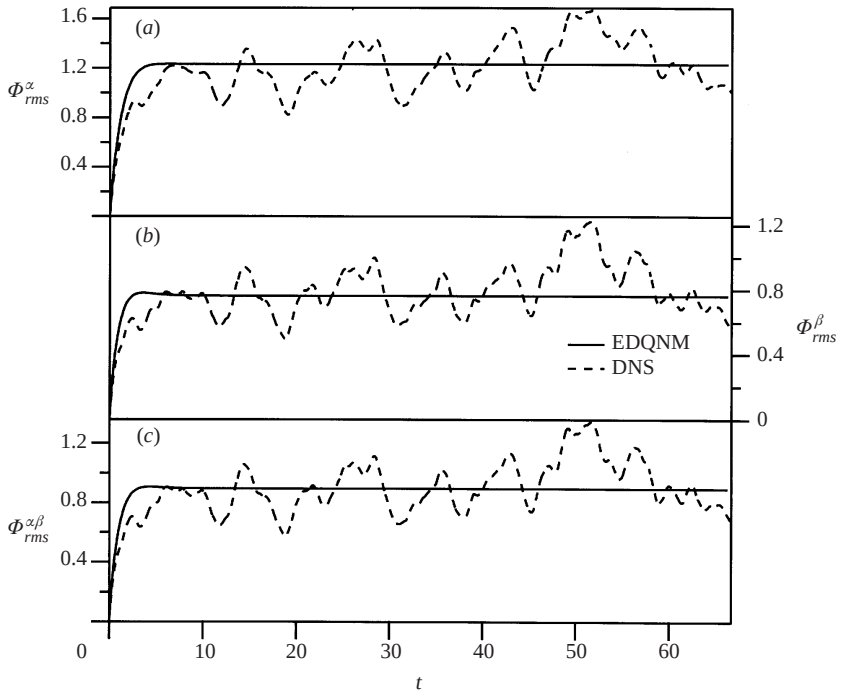

FIGURE 10. Scalar intensity (*a*) $\Phi^{\alpha}_{\rm rms}$, (*b*) $\Phi^{\beta}_{\rm rms}$ and (*c*) $\Phi^{\alpha\beta}_{\rm rms}$ as a function of dimensionless time for case (ii) of the mean gradient study.

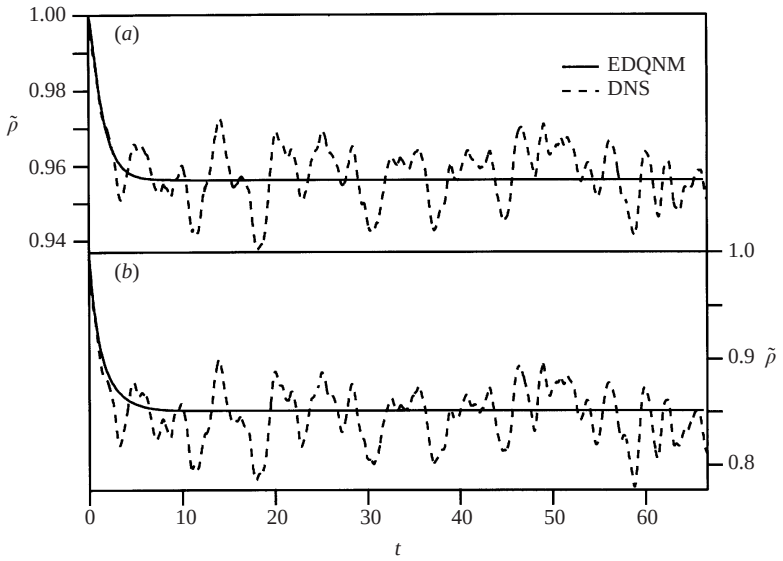

FIGURE 11. Correlation coefficient (see (2.36) for definition) as a function of time for two scalars with uniform mean gradients. (*a*) Case (i), (*b*) case (ii).

Case	DNS	EDQNM	% Error
$\Phi^{\alpha}_{\rm rms}(Sc=1)$	1.1737	1.2297	4.7
$\Phi^{\alpha}_{\rm rms}(Sc=\frac{1}{4})$	0.9915	1.0265	3.5
$\Phi^{\alpha}_{\rm rms}(Sc=\frac{1}{16})$	0.7700	0.7631	−0.9
$\Phi^{\alpha\beta}_{\rm rms}$ (case (i))	1.0556	1.0986	4.0
$\Phi^{\alpha\beta}_{\rm rms}$ (case (ii))	0.8748	0.8937	2.1
$\tilde{\rho}$ (case (i))	0.9575	0.9562	−0.1
$\tilde{\rho}$ (case (ii))	0.8459	0.8511	0.6
$-\overline{u_3'\phi_\alpha'}(Sc=1)$	0.5985	0.6049	1.0
$-\overline{u_3'\phi_\alpha'}(Sc=\frac{1}{4})$	0.5674	0.5569	−1.8
$-\overline{u_3'\phi_\alpha'}(Sc=\frac{1}{16})$	0.4872	0.4606	−5.0

TABLE 5. Comparison of averaged statistics from DNS with EDQNM model predictions for all of the single-point quantities in the mean gradient study.

uniform mean gradient. This can be explained in part by considering the relative contributions to the overall transfer in the EDQNM model by the various classes of terms (see § 6.2 for a more in-depth discussion of this point).

Figure 16 shows the coherency spectrum $\rho(k)$. We again observe a greater discrepancy for this statistic. However, the agreement is still reasonably good throughout the spectrum, and is surprisingly good for case (ii) with the more disparate Schmidt numbers.

4. Model for the covariance spectrum

An important consideration, from the perspective of practical calculations, is whether the covariance spectrum $E^{\alpha\beta}_{\phi}(k)$ can be represented purely in terms of an autocorrelation spectrum. There is no obvious relationship between $E^{\alpha\beta}_{\phi}(k)$ and the

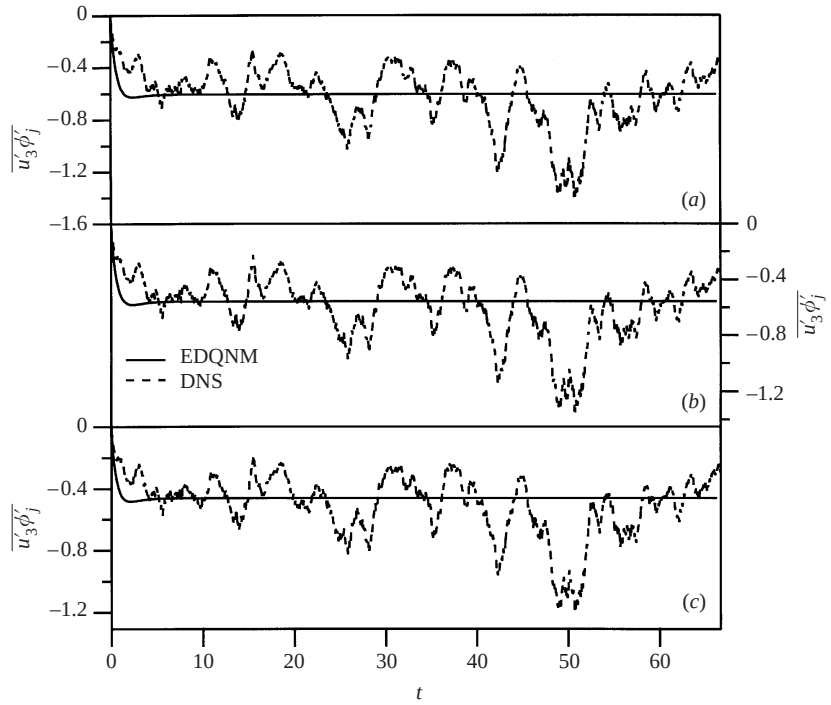

FIGURE 12. Turbulent scalar flux (see (2.35) for the definition). Schmidt number of (*a*) 1, (*b*) $\frac{1}{4}$ and (*c*) $\frac{1}{16}$.

Case	$\Phi^{\alpha\beta}_{\rm rms}$	$\Phi^{\gamma}_{\rm rms}$	Error
(i)	1.0986	1.0989	0.03%
(ii)	0.8937	0.8946	0.1%
(iii)	0.8627	0.8628	0.005%

TABLE 6. Comparison of $\Phi^{i}_{\rm rms}$ for the covariance spectrum with the autocorrelation spectrum of species γ with a molecular diffusivity equal to the arithmetic mean of the molecular diffusivities of species α and β.

two autocorrelation spectra, $E^{\alpha}_{\phi}(k)$ and $E^{\beta}_{\phi}(k)$, other than the Cauchy–Schwartz inequality that must be satisfied and that $E^{\alpha\beta}_{\phi}(k)$ must reduce properly to $E^{\alpha}_{\phi}(k)$ (or $E^{\beta}_{\phi}(k)$) when the two scalar diffusivities become equal. However, for the modified coefficients suggested by UC, it is possible to show that the EDQNM equation for $E^{\alpha\beta}_{\phi}(k)$ for an isotropic scalar reduces to the EDQNM equation for an autocorrelation spectrum $E^{\gamma}_{\phi}(k)$, where species γ has a molecular diffusivity that equals the arithmetic mean of the molecular diffusivities of species α and β (i.e. $\mathscr{D}_{\gamma} = (\mathscr{D}_{\alpha} + \mathscr{D}_{\beta})/2$, or equivalently, $Sc_{\gamma} = 2/(1/Sc_{\alpha} + 1/Sc_{\beta})$). This correspondence results from having a purely implicit dependence of the EDQNM expressions for the triple correlations on the scalar diffusivities.

The exact relationship for the isotropic covariance spectrum is only approximate in the case of a uniform mean gradient. Consequently, it is worth seeing how well $E^{\gamma}_{\phi}(k)$ approximates $E^{\alpha\beta}_{\phi}(k)$ for this case. Figure 17 shows a comparison of the steady-state

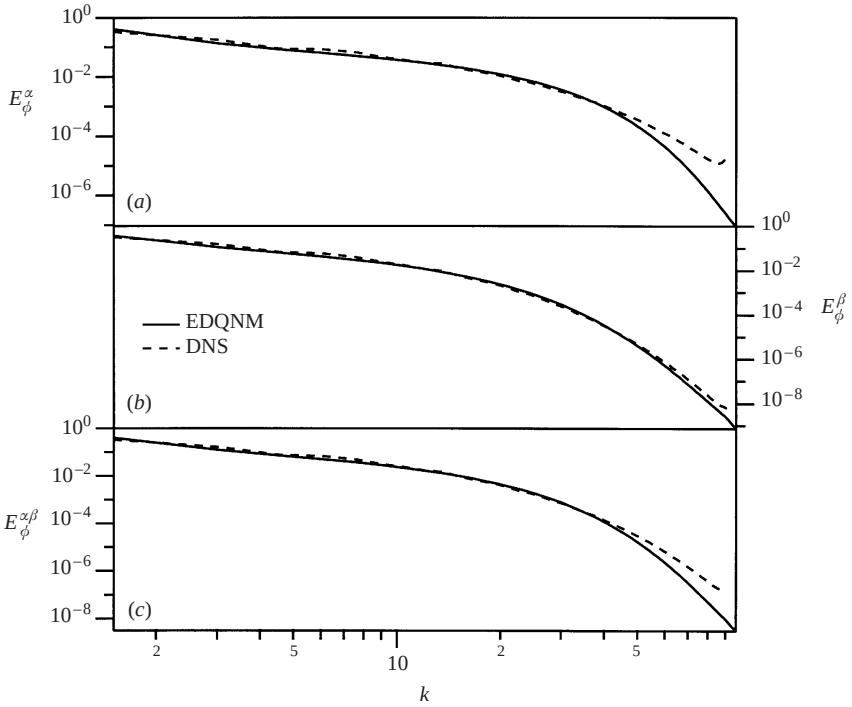

FIGURE 13. Scalar spectra for case (i) with the uniform mean gradient. (*a*) Autocorrelation spectra for (*a*) $Sc = 1$, (*b*) $Sc = \frac{1}{4}$ and (*c*) the scalar covariance spectrum.

spectra for $E^{\alpha\beta}_{\phi}(k)$ and $E^{\gamma}_{\phi}(k)$. The agreement is excellent over the entire spectrum. Table 6 shows a comparison of the single-point r.m.s. values for the two spectra. Notice that the maximum relative error for all cases is much less than 1%. The figures presented in this section strongly suggest that over the range of Schmidt numbers considered, we can interpret the effects of differential diffusion of inert species in terms of the ordinary diffusion of an appropriately defined single species.

5. Reynolds number scaling

We now are in a position to consider the dependence of differential diffusion on the Reynolds number. Earlier studies (e.g. Kerstein *et al.* 1989; Smith *et al.* 1995*a*, Nilsen & Kosály 1997; Saylor & Sreenivasan 1998) have consistently shown that the effect decreases with increasing Reynolds number. Here we address this question for $\tilde{\rho}$ and $\rho(k)$ using the EDQNM model.

5.1. *Scaling for* $\tilde{\rho}$

EDQNM calculations of the scalar with a uniform mean gradient were performed at the Reynolds numbers given in figure 18. We observe (not shown) that $\tilde{\rho}$ approaches unity with increasing Reynolds number, suggesting we should scale $1 - \tilde{\rho}$ with the Reynolds number. Empirically, we find that $(1 - \tilde{\rho}) \propto 1/Re_{\lambda}$ at high Re_{λ}. This is evident in figure 19, which shows $(1 - \tilde{\rho})Re_{\lambda}$ as a function of Re_{λ}. Notice that at high Reynolds numbers this quantity approaches a straight line, confirming the proposed scaling.

An explanation for this behaviour can be found by considering a simple approxi-

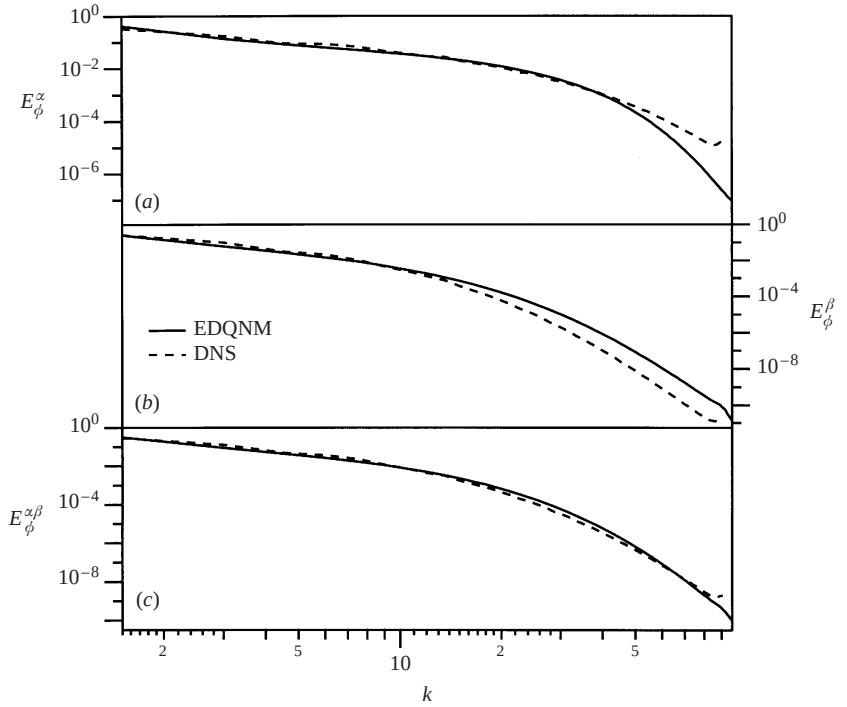

FIGURE 14. Scalar spectra for case (ii) with the uniform mean gradient. (*a*) Autocorrelation spectra for $Sc = 1$, (*b*) $Sc = \frac{1}{16}$ and (*c*) the scalar covariance spectrum.

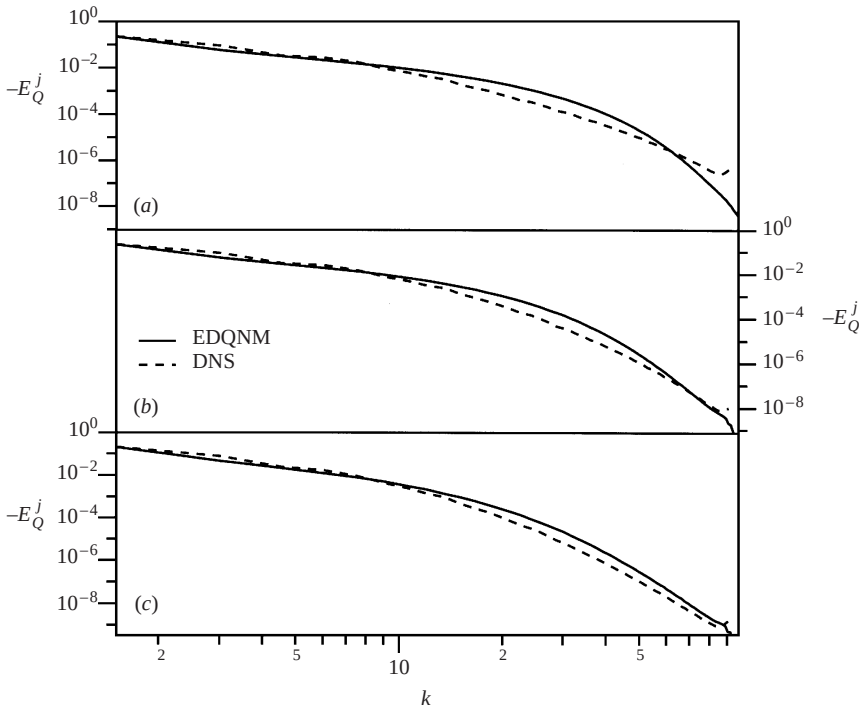

FIGURE 15. Scalar velocity spectrum, $E^{j}_{Q}(k)$, for a Schmidt number of (*a*) 1, (*b*) $\frac{1}{4}$ and (*c*) $\frac{1}{16}$.

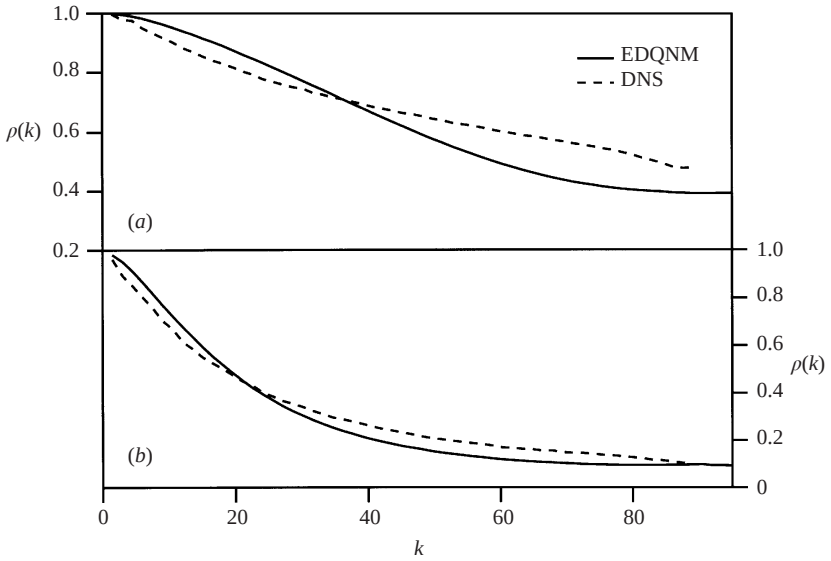

FIGURE 16. Coherency spectrum $\rho(k)$ for (a) case (i) and (b) case (ii) of the uniform mean gradient study.

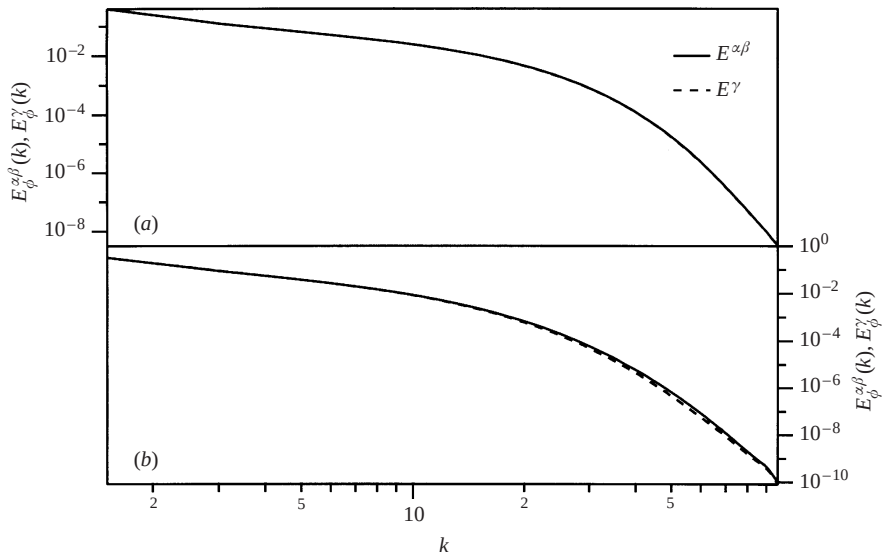

FIGURE 17. Steady state scalar covariance spectrum $E_\phi^{\alpha\beta}(k)$ and the autocorrelation spectrum $E_\phi^{\gamma}(k)$ for the species γ with a molecular diffusivity equal to the arithmetic mean of the diffusivities of species α and β. (a) Case (i), (b) case (ii).

mation to the scalar spectrum. Batchelor, Howells & Townsend (1959) showed that the Oboukov–Corrsin $k^{-5/3}$ spectrum is followed by a $k^{-17/3}$ range in the so-called inertial–conductive range. According to the classical scaling argument, this range of wavenumbers is defined as: $k_\alpha \leqslant k \leqslant k_\eta$, where $k_\alpha \equiv Sc_\alpha^{3/4} k_\eta$, and this range exists only for $Sc_\alpha < 1$. A simple (dimensional) scalar spectrum that obeys this scaling can

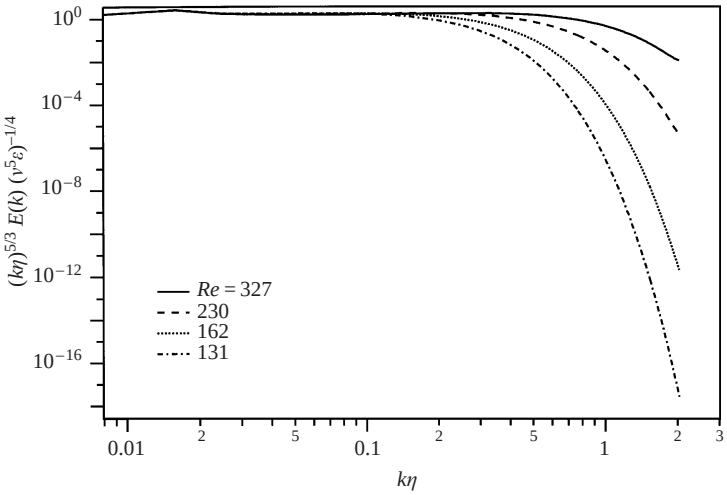

FIGURE 18. Energy spectra calculated from the EDQNM model at Reynolds numbers (based on the Taylor microscale) of: (i) 327, (ii) 231, (iii) 162 and (iv) 131.

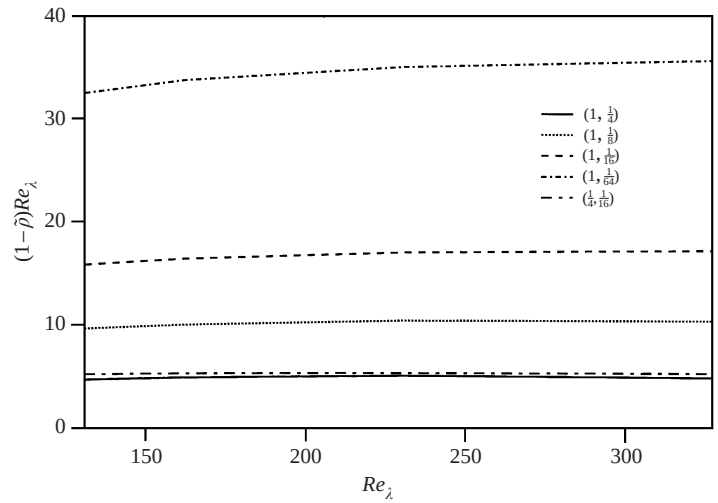

FIGURE 19. Steady state $(1-\tilde{\rho})Re_\lambda$ versus Re_λ. Notice the curves become flat at high Reynolds number.

be defined as follows:

$$E_\phi^\alpha(k) \approx C\chi_\alpha \epsilon^{-1/3} k^{-5/3} \exp(-\delta k/k_\alpha) f(\epsilon, \mathscr{D}_\alpha, k), \tag{5.1}$$

where δ is a non-dimensional constant that determines the onset of the exponential tail at high wavenumbers (in general, we assume $\delta \ll 1$ and expand the solution to $O(\delta)$), C is the Oboukov–Corrsin constant,

$$f(\epsilon, \mathscr{D}_\alpha, k) \equiv \begin{cases} 1, & k_0 \leqslant k \leqslant k_\alpha, \\ \dfrac{\epsilon}{\mathscr{D}_\alpha^3 k^4}, & k_\alpha < k < \infty, \end{cases} \tag{5.2}$$

and k_0 is the inverse of the integral scale of the turbulence. In the limit of high Reynolds number, $C = \frac{4}{9}$ ensures that (5.1) is consistent with $\chi_\alpha = 2\mathscr{D}_\alpha \int_0^\infty k^2 E_\phi^\alpha(k)\,\mathrm{d}k$.

Case	Equation (5.6)	EDQNM model	Difference
(i)	0.800	0.816	2%
(ii)	0.471	0.481	2.1%
(iii)	0.800	0.800	0%

TABLE 7. Comparison of the approximation for $g_{\alpha\beta}$ by Yeung (1998) with our EDQNM results.

The simple analytical expression shown in (5.1) enables us to calculate $\Phi^{\alpha}_{\rm rms}$ and $\Phi^{\beta}_{\rm rms}$. Furthermore, if we use the approximation discussed in §4, we can obtain an expression for $\Phi^{\alpha\beta}_{\rm rms}$, and thereby derive a formula for $\tilde{\rho}$. The resulting expression is

$$\tilde{\rho} \approx \frac{\tilde{\rho}_\chi \left(1 - \frac{6}{7}\frac{\sqrt{15}p^{2/3}}{Re_\lambda\sqrt{Sc_{\alpha\beta}}}\right)}{\left(1 - \frac{6}{7}\frac{\sqrt{15}p^{2/3}}{Re_\lambda\sqrt{Sc_\alpha}}\right)^{1/2}\left(1 - \frac{6}{7}\frac{\sqrt{15}p^{2/3}}{Re_\lambda\sqrt{Sc_\beta}}\right)^{1/2}}, \tag{5.3}$$

where $Re_\lambda \equiv u'^2\sqrt{15/\nu\epsilon}$, $Sc_{\alpha\beta} \equiv 2/(1/Sc_\alpha + 1/Sc_\beta)$, $\tilde{\rho}_\chi \equiv \chi_{\alpha\beta}/\sqrt{\chi_\alpha\chi_\beta}$ and p is the proportionality constant

$$p \equiv \frac{k_0 u'^3}{\epsilon}. \tag{5.4}$$

The EDQNM model predicts $p = \frac{8}{3}$ at high Reynolds numbers. The coefficient $\tilde{\rho}_\chi$ is a correlation coefficient for the scalar dissipation. Yeung (1998) has an extensive discussion of a related coefficient defined as

$$g_{\alpha\beta} \equiv \frac{\overline{\nabla\phi'_\alpha \cdot \nabla\phi'_\beta}}{\sqrt{\overline{\nabla\phi'_\alpha \cdot \nabla\phi'_\alpha}\;\overline{\nabla\phi'_\beta \cdot \nabla\phi'_\beta}}}, \tag{5.5}$$

which at steady state he approximates as

$$g_{\alpha\beta} = \frac{2\sqrt{Sc_\alpha Sc_\beta}}{(Sc_\alpha + Sc_\beta)}. \tag{5.6}$$

Table 7 shows a comparison of the EDQNM prediction for $g_{\alpha\beta}$ with the approximation shown in (5.6). The agreement is within 3% for all cases considered. Combining this approximation for $g_{\alpha\beta}$ with the definitions given in (2.2)–(2.4), we conclude that $\tilde{\rho}_\chi \approx 1$ and ignore it in what follows.

It is possible to predict the leading-order Reynolds number scaling of (5.3) by making a Taylor series expansion in powers of $1/Re_\lambda$. After some manipulation, it can be shown that

$$(1 - \tilde{\rho})Re_\lambda \simeq \frac{3\sqrt{15}p^{2/3}}{7}\left(\frac{2}{\sqrt{Sc_{\alpha\beta}}} - \frac{1}{\sqrt{Sc_\alpha}} - \frac{1}{\sqrt{Sc_\beta}}\right) + O(Re_\lambda^{-1}), \tag{5.7}$$

which is consistent with the scaling observed for the EDQNM model (see figure 19). It is also worth noting that a similar scaling was predicted by Kerstein *et al.* (1995). They defined a difference variable $z \equiv \phi_\alpha - \phi_\beta$ and considered the statistics of $\overline{z'^2}$. If

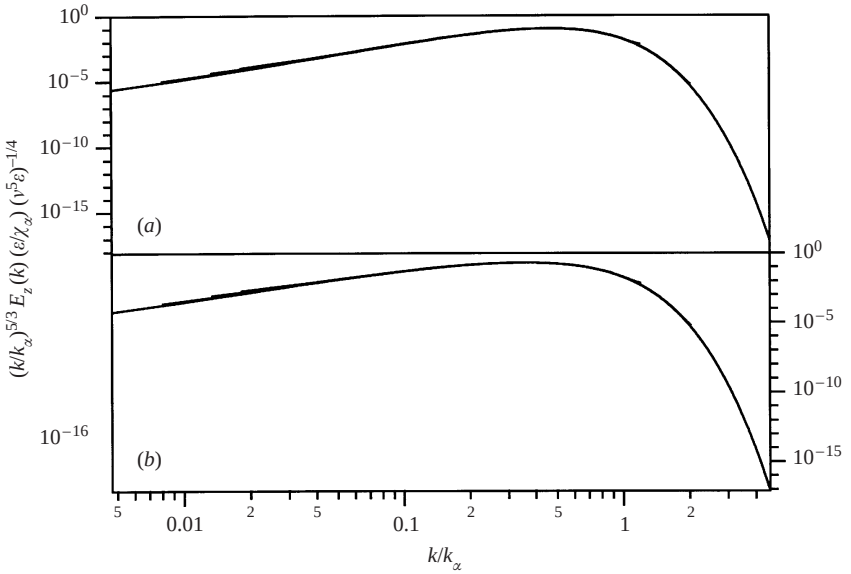

FIGURE 20. Compensated spectrum for $z \equiv \phi_\alpha - \phi_\beta$ plotted against k/k_α for (a) case (i) and (b) case (ii) at the Reynolds numbers given in the caption of figure 18. Notice that the curves corresponding to the different Reynolds numbers collapse onto a single curve in this coordinate.

we again use (5.3) to model $\overline{z'^2}$, we obtain

$$\begin{aligned}\overline{z'^2} &\equiv (\Phi^\alpha_{\rm rms})^2 + (\Phi^\beta_{\rm rms})^2 - 2(\Phi^{\alpha\beta}_{\rm rms})^2 \\ &= \frac{6\sqrt{15}p^{2/3}}{7Re_\lambda}\left(\frac{2}{\sqrt{Sc_{\alpha\beta}}} - \frac{1}{\sqrt{Sc_\alpha}} - \frac{1}{\sqrt{Sc_\beta}}\right)\frac{3C\chi_\alpha}{2\epsilon^{1/3}k_0^{2/3}} + O(Re_\lambda{}^{-2}) \\ &= (1-\tilde{\rho})\frac{3C\chi_\alpha}{\epsilon^{1/3}k_0^{2/3}} + O(Re_\lambda{}^{-2}). \end{aligned} \tag{5.8}$$

Thus, $\overline{z'^2}$ scales like $(1-\tilde{\rho})$, approaching zero like $Re_\lambda{}^{-1}$, which is consistent with their prediction of $Re_L{}^{-1/2}$, since $Re_\lambda \propto Re_L{}^{1/2}$.

The numerical values predicted by (5.3) are not in quantitative agreement with the EDQNM model (e.g. off by factors of 5–10); however, this is not to be expected given the simple approximation for the scalar spectrum we used (see (5.1)).

5.2. *Scaling relationships for scalar spectra*

We now consider Reynolds-number scaling relationships for scalar spectra. Yeung (1998) hypothesized that the scalar spectrum for the concentration difference, z, would collapse in the inertial range if the compensated spectrum, $(k/k_\alpha)^{5/3}E_z(k)(\epsilon/\chi_\alpha)(\nu^5\epsilon)^{-1/4}$ were plotted against k/k_α, where $E_z(k)$ is the spectrum for z, and species α is assumed to be the more slowly diffusing species. This hypothesis is tested in figure 20, which shows compensated spectra for cases (i) and (ii) at the four Reynolds numbers given in figure 18. Notice that the curves collapse in this coordinate over all wavenumbers, in agreement with Yeung (1998). However, the two curves corresponding to cases (i) and (ii) do not collapse together; that is, each combination of Schmidt numbers yields a distinct curve.

Figure 21 shows an equivalent plot of the coherency spectrum as a function of $k\eta$,

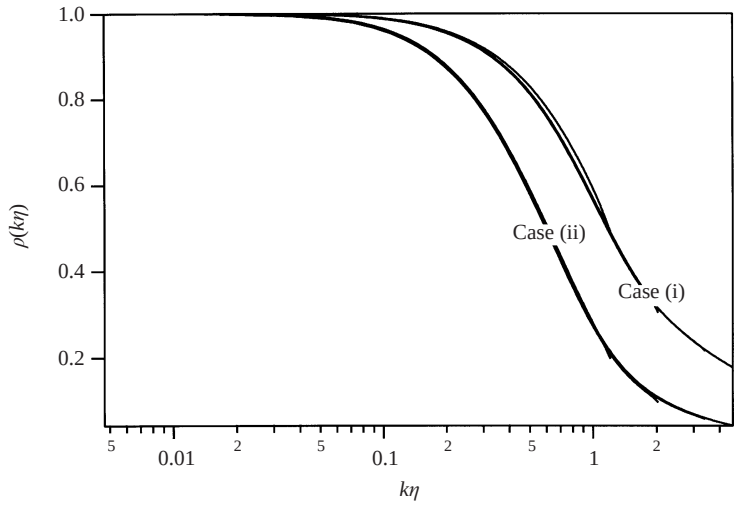

FIGURE 21. Coherency spectra at different Reynolds numbers for cases (i) and (ii).

the suggested scaling by Yeung. Once again, the curves at different Reynolds numbers collapse, but the curves for the two cases remain distinct. The results suggest that we should seek a scaling argument that accounts for the Schmidt-number dependence in each curve. To that end, Yeung (1998) proposed the following decomposition of the coherency spectrum

$$\rho(k\eta) = 1 - f_1(k\eta) f_2(Sc_\alpha, Sc_\beta). \tag{5.9}$$

The decomposition implies that each portion of the spectrum is affected uniformly by any changes to the Schmidt number. This hypothesis can be tested directly. If we define $\rho^{(i)}(k\eta)$ and $\rho^{(ii)}(k\eta)$ as the collapsed curves corresponding to cases (i) and (ii), respectively, in figure 21, then (5.9) implies that the function

$$\Lambda = \frac{[1 - \rho^{(i)}(k\eta)]}{[1 - \rho^{(ii)}(k\eta)]} = \frac{f_2(1, \frac{1}{4})}{f_2(1, \frac{1}{16})} \tag{5.10}$$

should be independent of $k\eta$. Figure 22 shows a graph of Λ versus $k\eta$; it is readily apparent that Λ is a strong function of wavenumber, implying that the decomposition shown in (5.9) is not valid. Apparently, an intermediate circumstance arises, in which we can make the weaker claim

$$\rho(k\eta) = 1 - f(k\eta, Sc_\alpha, Sc_\beta), \tag{5.11}$$

where f is independent of Reynolds number.

6. Transfer spectra

The agreement between the EDQNM predictions for the scalar spectra and the DNS provides confidence that the model reliably represents the triple correlations that lead to transfer of the scalar (principally) from lower to higher wavenumbers. A natural question to consider is whether the dominant mechanism of transfer is local or non-local. Local transfer can be represented by a far simpler differential expression that would eliminate the need for the convolution integral, and thus would be more efficient to solve. Additionally, the form of the transfer term for anisotropic scalars involves several classes of terms with widely-varying magnitudes. A second question

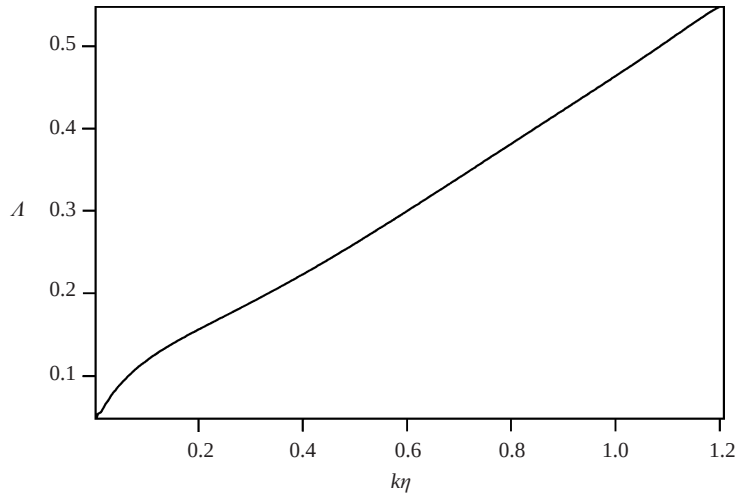

FIGURE 22. Coherency spectrum ratio (Λ) defined in (5.10) versus $k\eta$.

to consider is the relative contribution of the different terms to the overall transfer function.

The overall transfer function for $E_\phi^{\alpha\beta}(k)$, denoted by $Tr^{\alpha\beta}(k)$, is given by

$$Tr^{\alpha\beta}(k) = \frac{k^2}{4\pi^2}\int_{-1}^{1}\left[-k_j\int\!\!\int (M_j^{\alpha\beta}(\boldsymbol{p},\boldsymbol{k},\boldsymbol{q}) + M_j^{\beta\alpha}(\boldsymbol{p},\boldsymbol{k},\boldsymbol{q}))\,\hat{\mathrm{d}}\boldsymbol{p}\,\hat{\mathrm{d}}\boldsymbol{q}\right]\mathrm{d}\mu. \tag{6.1}$$

Equations for $Tr^{\alpha}(k)$ and $Tr^{\beta}(k)$ follow by contracting α or β. The double integral in (6.1) can be thought of as summing the contributions from all of the possible triads. Although we can consider all three transfer spectra, hereinafter we will focus on the one given in (6.1); however, the results for $Tr^{\alpha}(k)$ and $Tr^{\beta}(k)$ are in close qualitative agreement with $Tr^{\alpha\beta}(k)$. Thus, all conclusions that we draw hold equally well for these spectra.

To facilitate making comparisons, it is convenient to define a transfer flux as

$$\Pi(k) = \int_k^{k_{\max}} Tr^{\alpha\beta}(k')\,\mathrm{d}k'. \tag{6.2}$$

An important advantage of $\Pi(k)$ is that it is positive definite for all k.

6.1. *Local vs. non-local transfer*

Whether the transfer process is local or non-local in nature is a difficult point in the turbulence literature, because local triadic interactions result in local transfer, whereas non-local interactions can result in either local or non-local transfer (Domaradzki & Rogallo 1990; Zhou 1993*a*,*b*; Brasseur & Wei 1994). The problem of characterizing transfer is especially difficult for the case of energy transfer, where interactions occur among the three velocity modes of the triad; however, for scalar transfer, the corresponding triads only exchange scalar between two of the three legs of the triad (the velocity leg serving only to control the rate of exchange). This is illustrated in figure 23, which shows a schematic of three typical triads. The first represents nearly equilateral triads that result in local interactions that lead to local transfer. The second and third examples are of non-local interactions producing local and non-local transfer, respectively. As can be seen, the signature of non-local transfer

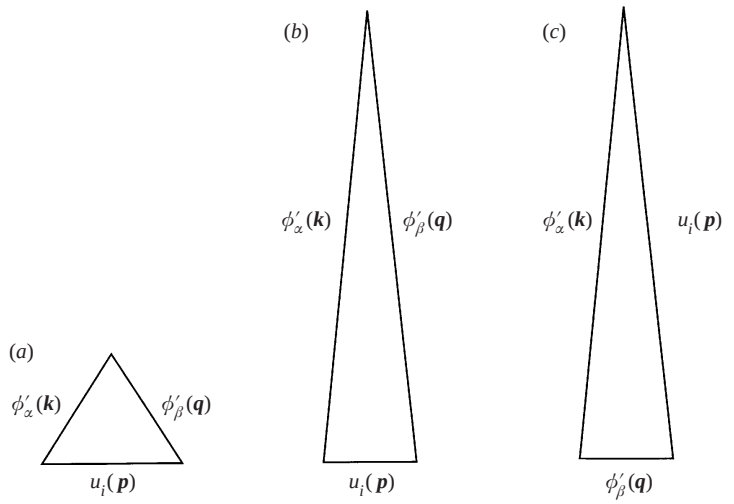

FIGURE 23. Schematic of (*a*) local triadic interaction leading to local transfer, (*b*) non-local triadic interaction leading to local transfer and (*c*) non-local triadic interaction leading to non-local transfer. Notice that non-local transfer requires that the velocity mode of the triad comes from the high wavenumber end of the energy spectrum.

will be long skinny triads having an interaction between the velocity at a relatively high wavenumber with scalar at both low and high wavenumbers. If we can show that this contribution is relatively small, then we have an intermediate situation in which non-local triadic interactions lead to local scalar transfer.

The above qualitative arguments suggest that we can gain insight into the question of local versus non-local transfer by breaking the energy spectrum into different ranges. Here, we break the spectrum into three different ranges corresponding to k between the first wavenumber and the Taylor microscale (range 1), k between the Taylor microscale and the Kolmogorov scale (range 2), and k between the Kolmogorov scale and $k_{\max}$. The numerical values for the ranges in dimensionless form are

$$\text{range 1:} \quad 1.51 \leqslant k < 9.05,$$

$$\text{range 2:} \quad 9.05 \leqslant k < 319.70,$$

$$\text{range 3:} \quad 319.70 \leqslant k < 386.05.$$

We recognize from the outset that the above divisions are arbitrary, reflecting the arbitrariness of the division between 'local' and 'non-local' transfer. Others such as Yeung (1996) have used finer-grained divisions to divide the energy. However, the major qualitative findings will not be affected by the choice of the divisions.

It is now possible to consider the contribution to the total transfer from triads with energy legs lying within each of the ranges. Based on the above definitions, we define a fractional contribution to the covariance spectrum flux resulting from each of the wavenumber bands as

$$\Pi_m(k) = \frac{\displaystyle\int_k^{k_{\max}} Tr_m^{\alpha\beta}(k')\,\mathrm{d}k'}{\Pi(k)}, \tag{6.3}$$

where $Tr_m^{\alpha\beta}(k)$ is the transfer of the covariance spectrum associated with the mth range ($m = 1$, 2 or 3) and $\Pi_m(k)$ is the fractional contribution of the mth range to

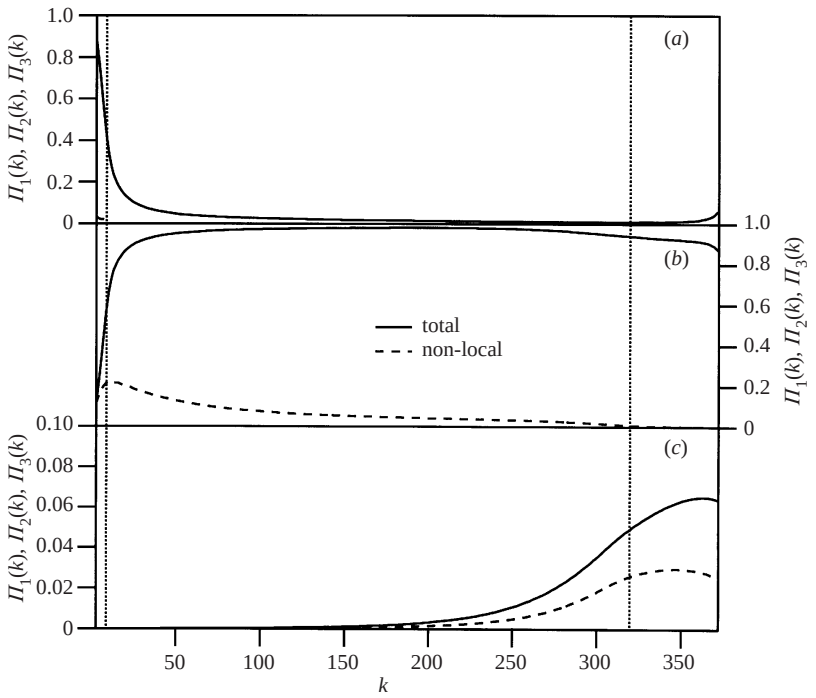

FIGURE 24. Normalized steady state state flux spectra resulting from the three regions of the energy spectrum for case (i) (note: see (6.3) for the definition of the flux spectrum). (*a*) $\Pi_1(k)$, (*b*) $\Pi_2(k)$ and (*c*) $\Pi_3(k)$. The dashed line in each graph shows the contribution from non-local transfer, here defined as triads with the ratio of scalar legs greater than a factor of 5. Vertical lines indicate the transitions between the different regions. Notice that the range of the ordinate of the bottom graph is much smaller than the other two graphs.

the flux (note that by definition $\Pi_1(k) + \Pi_2(k) + \Pi_3(k) = 1$). We further define the contribution to $\Pi_m(k)$ from non-local interactions, here chosen as triads with the ratio of the scalar legs that is greater than a factor of 5.

Figures 24 and 25 show the mean gradient results for cases (i) and (ii). At low wavenumbers, it is clear that $\Pi_1(k)$ and $\Pi_2(k)$ dominate ranges 1 and 2, respectively, and the contribution from $\Pi_3(k)$ is negligible for both of the cases. Transfer over these two ranges is controlled principally by the energy within each respective range. In contrast, transfer within range 3 is predominantly from $\Pi_2(k)$, although there is an appreciable contribution from $\Pi_3(k)$. It appears that local interactions and hence local transfer are dominant in ranges 1 and 2, but non-local interactions are important in range 3.

Next, we consider whether these non-local interactions lead to local or non-local transfer. According to the qualitative picture shown in figure 23, non-local interactions can lead to both local and non-local transfer. The signature for non-local scalar transfer is interactions between an energy leg at relatively high wavenumbers with scalar legs at low and high wavenumbers, respectively. We examine the importance of non-local transfer for each Π-group in figures 24 and 25 (dashed lines). Notice that non-local transfer is negligible in ranges 1 and 2, in agreement with the fact that local interactions are dominant. Range 3 has a significant contribution from $\Pi_2(k)$; however, the fraction of the contribution that is non-local is negligible for both cases. This strongly suggests that non-local interactions leading to local transfer

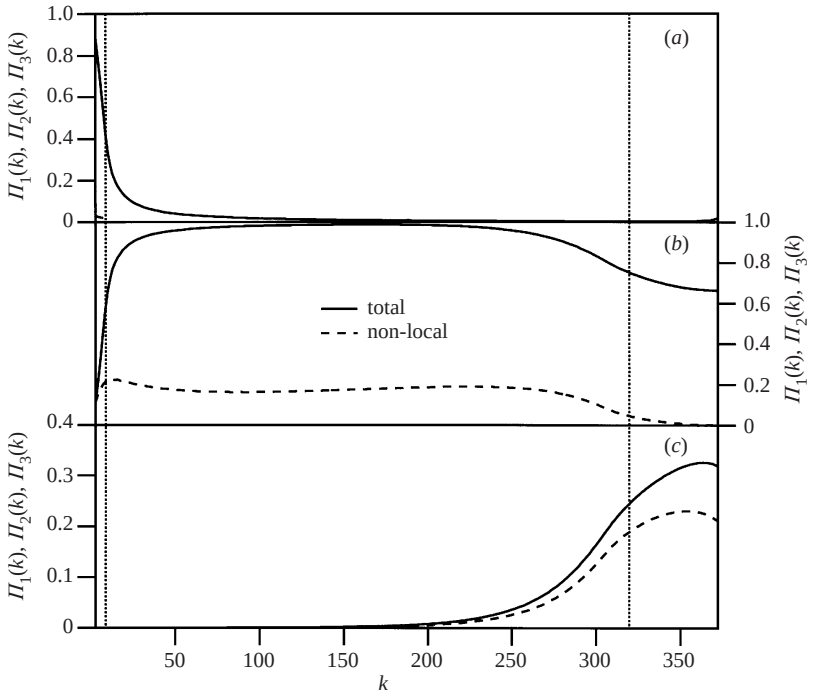

FIGURE 25. Same as figure 24, except for case (ii).

are important. The non-local fraction of $\Pi_3(k)$ in range 3 is appreciable, implying that there is some non-local transfer in this range.

To summarize, the EDQNM model demonstrates that scalar transfer is dominated first by local interactions (local transfer) followed by non-local interactions that lead to local transfer. Non-local interactions that lead to non-local transfer are only important in range 3. This has important implications for developing simpler spectral models. For example, there have been a number of spectral energy models based on local transfer mechanisms (Besnard *et al.* 1996; Leith 1967). Our results suggest that their approach can be extended to the scalar spectrum as well, supporting the recent work by Fox (1995, 1997); however, the significant contribution that we observe from non-local interactions indicates that the flux at a particular wavenumber k could depend upon the energy spectrum in the neighbourhood of k (and not solely the energy at k). Generalizations of local models that preserve their computational simplicity yet account for these non-local interactions can be easily envisaged. For example, weighted integrals of the energy spectrum can be substituted for the local energy value so as to spread the influence of the energy spectrum appropriately.

6.2. *Breakdown of interactions*

As shown in § 2.2, the presence of the mean scalar gradient introduces several new interactions into the transfer function $M_i^{\alpha\beta}(\boldsymbol{k},\boldsymbol{p},\boldsymbol{q})$. For the sake of computational economy, it is again useful to consider the relative contributions of each interaction to the overall scalar transfer rate. In order to determine which, if any, of the spectral interactions dominate the transfer of $E_\phi^{\alpha\beta}(k)$, it is necessary to break up the equation for $M_i^{\alpha\beta}(\boldsymbol{k},\boldsymbol{p},\boldsymbol{q})$ into its constitutive parts. Equation (2.30) and table 1 show that the interactions that compose $M_i^{\alpha\beta}(\boldsymbol{k},\boldsymbol{p},\boldsymbol{q})$ are $B^{\alpha\beta}R$, $Q^\alpha Q^\beta$, $Q^\alpha R$, $Q^\beta R$ and RR. To

facilitate the comparison, we decompose the total scalar flux in the following manner

$$\Pi_{RR}(k) \equiv \frac{\int_k^{k_{\max}} Tr_{RR}^{\alpha\beta}(k')\,\mathrm{d}k'}{\Pi(k)}, \tag{6.4}$$

$$\Pi_{QR}(k) \equiv \frac{\int_k^{k_{\max}} Tr_{QR}^{\alpha\beta}(k')\,\mathrm{d}k'}{\Pi(k)}, \tag{6.5}$$

$$\Pi_{QQ}(k) \equiv \frac{\int_k^{k_{\max}} Tr_{QQ}^{\alpha\beta}(k')\,\mathrm{d}k'}{\Pi(k)}, \tag{6.6}$$

$$\Pi_{BR}(k) \equiv \frac{\int_k^{k_{\max}} Tr_{BR}^{\alpha\beta}(k')\,\mathrm{d}k'}{\Pi(k)}, \tag{6.7}$$

where $Tr_{RR}^{\alpha\beta}$ is the contribution to the overall transfer from the RR terms, $Tr_{QR}^{\alpha\beta}(k)$ is the contribution from the $Q^\alpha R$ and $Q^\beta R$ terms, $Tr_{QQ}^{\alpha\beta}(k)$ is the contribution from $Q^\alpha Q^\beta$ terms, and $Tr_{BR}^{\alpha\beta}(k)$ is the contribution from $B^{\alpha\beta}R$ terms.

Figure 26 shows the breakdown of the scalar flux as a function of wavenumber for cases (i) and (ii). The dominant interaction for both cases is BR, followed by QR, which is significant at low wavenumbers. The contributions from the other interactions are much smaller, and can be neglected in a simplified spectral model.

6.3. *Backscatter coefficient*

Fox (1999) extended the spectral relaxation model to account for differential diffusion by introducing backscatter into the original formulation. Fox reasoned that backscatter is responsible for the inverse cascade of 'incoherence' that is initiated at high wavenumbers by differential diffusion. To account for this, Fox defined a coefficient that determines the rate of backscatter. Here, we will calculate the backscatter coefficient using the EDQNM model.

To begin, we first decompose the total transfer function defined in (6.1) into forward and reverse transfer as follows:

$$Tr^{>}(k) = \frac{k^2}{2\pi^2}\int_{-1}^{1}\left[-k_j\iint M_j^\alpha(\boldsymbol{p},\boldsymbol{k},\boldsymbol{q})H(k-q)\,\hat{\mathrm{d}}\boldsymbol{p}\,\hat{\mathrm{d}}\boldsymbol{q}\right]\mathrm{d}\mu, \tag{6.8}$$

$$Tr^{<}(k) = \frac{k^2}{2\pi^2}\int_{-1}^{1}\left[-k_j\iint M_j^\alpha(\boldsymbol{p},\boldsymbol{k},\boldsymbol{q})H(q-k)\,\hat{\mathrm{d}}\boldsymbol{p}\,\hat{\mathrm{d}}\boldsymbol{q}\right]\mathrm{d}\mu, \tag{6.9}$$

where $Tr^{>}(k)$ is forward transfer, $Tr^{<}(k)$ is reverse transfer and $H(x)$ is the Heaviside or unit step function. (Note that all of the discussion will focus on the autocorrelation transfer spectrum only; however, the concepts can be extended easily to the covariance spectrum.) By definition, we immediately recover that $Tr^{\alpha}(k) = Tr^{>}(k) + Tr^{<}(k)$. The backscatter coefficient is then defined in terms of the reverse transfer function (Fox 1999)

$$\beta_D \equiv \frac{-0.5\int_{k_D}^{\infty} Tr^{<}(k)\,\mathrm{d}k}{\int_{k_D}^{\infty} E_\phi^\alpha(k)\,\mathrm{d}k}, \tag{6.10}$$

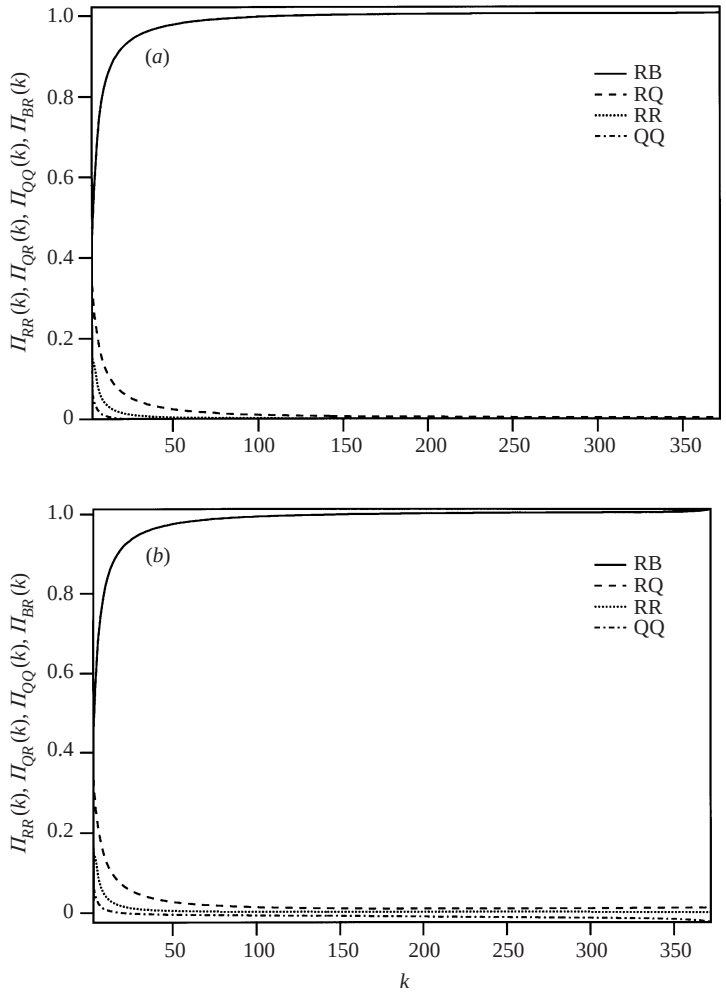

FIGURE 26. Fractional contribution of the different spectral interactions to the total flux of the scalar covariance spectrum for (*a*) case (i) and (*b*) case (ii).

where k_D defines the beginning of the dissipation range. Classical scaling yields $k_D = k_\alpha$; however, Fox & Yeung (1999) propose the following implicit formula for k_D

$$\frac{\left(\int_{k_D}^{\infty} E_\phi^\alpha(k)\,\mathrm{d}k\right)\left(\int_{k_D}^{\infty} k^4 E_\phi^\alpha(k)\,\mathrm{d}k\right)}{\left(\int_{k_D}^{\infty} k^2 E_\phi^\alpha(k)\,\mathrm{d}k\right)^2} = C_d, \tag{6.11}$$

where k_D is adjusted until (6.11) is satisfied. The value of C_d is uncertain, with Fox & Yeung (1999) suggesting $\frac{5}{3}$ and Vedula, Yeung & Fox (2001) suggesting 3. The quantitative values are sensitive to the choice of C_d, but the trends are relatively insensitive. For the sake of this discussion, we have fixed its value at $C_d = \frac{5}{3}$.

The results for β_D obtained from the EDQNM model with standard and UC-modified coefficients are summarized in table 8. Results from DNS are shown for comparison. It is apparent that while the UC-modified EDQNM model obtains the

Schmidt number	Modified	Standard	DNS
1	3.00	3.00	8.00
$\frac{1}{4}$	2.70	1.45	3.50
$\frac{1}{16}$	3.10	0.62	1.57

TABLE 8. Comparison of the β_D for the autocorrelation spectrum predicted by the UC-modified EDQNM model, the standard EDQNM model and DNS at the specified values of Schmidt number.

correct order of magnitude, it does not capture the Schmidt-number dependence observed in the DNS. Fox & Yeung (1999) found the coefficient to be proportional to $Sc_\alpha^{1/2}$, in agreement with our DNS, but the UC-modified model predicts essentially no dependence on Schmidt number. It is interesting to note that the standard EDQNM model captures the Schmidt number dependence more accurately.

A closer examination of the numerator and denominator of β_D (see (6.10)) shows that most of the error is associated with the reverse transfer function. Figure 27 shows comparisons of the two EDQNM models with the DNS. Notice that the standard model predicts the trend with Schmidt number more consistently.

Even though the modified EDQNM model does not capture backscatter as well as the standard (unrealizable) model, we see in figure 28 that the overall transfer is very well described by the modified model. This figure shows a comparison of the total transfer function at three Schmidt numbers with DNS. Apparently, the modifications proposed by UC to eliminate the realizability problem do adversely affect the prediction of backscatter, but not the prediction of total transfer.

7. Conclusions

The EDQNM theory has been used to investigate differential diffusion of non-reacting species in stationary isotropic turbulence. The advantage of a spectral description of differential diffusion is that the effects due to interactions between the hydrodynamic and scalar fields at different length scales are inherently accounted for. Several single- and two-point statistics were used to examine both the transient and steady-state behaviour of the scalar field. From these statistics, we observed that differential diffusion is a molecular phenomenon that originates at the smallest length scales and whose effects are more pronounced as the ratio of the Schmidt numbers increases. We have seen that differential diffusion acts as a sink of coherency at the small scales, causing them to decorrelate very quickly, whereas the mean scalar gradient acts as a source term for coherency at the large scales. Thus, there is a competition between the source and sink of coherency, resulting in a mixture that depends on the wavenumber, the Reynolds number and the two scalar Schmidt numbers.

Comparisons of the modified EDQNM model with DNS were presented for a broad range of Schmidt numbers. Overall, the agreement for single-point and spectral statistics, both with and without a uniform mean gradient, was very good. A slight modification of one of the coefficients, c_{2T}, improved the performance of the model for the scalar with the mean gradient. The least agreement was found for the coherency spectrum, $\rho(k)$. As this quantity involves a ratio of scalar spectra, it is a particularly sensitive test. Thus, the acceptable agreement achieved with this statistic implies the model for the individual spectra is performing very well. We also showed that the

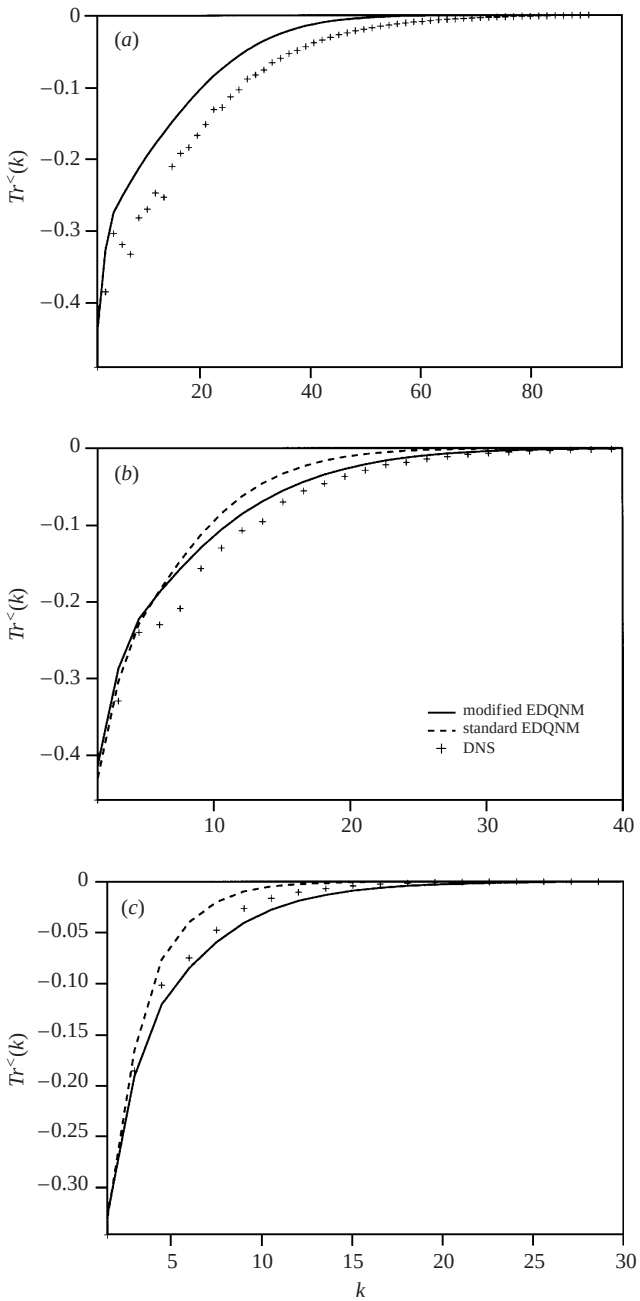

FIGURE 27. Backscatter transfer function predicted by the EDQNM model with modified coefficients (UC), EDQNM model with standard coefficients and the results from the DNS at Schmidt numbers (*a*) 1, (*b*) $\frac{1}{4}$ and (*c*) $\frac{1}{16}$.

scalar covariance spectrum can be modelled by the autocorrelation of a third scalar with a molecular diffusivity equal to the arithmetic mean of the diffusivities of the original two scalars. Single-point statistics were predicted to less than 1% error by this approximation.

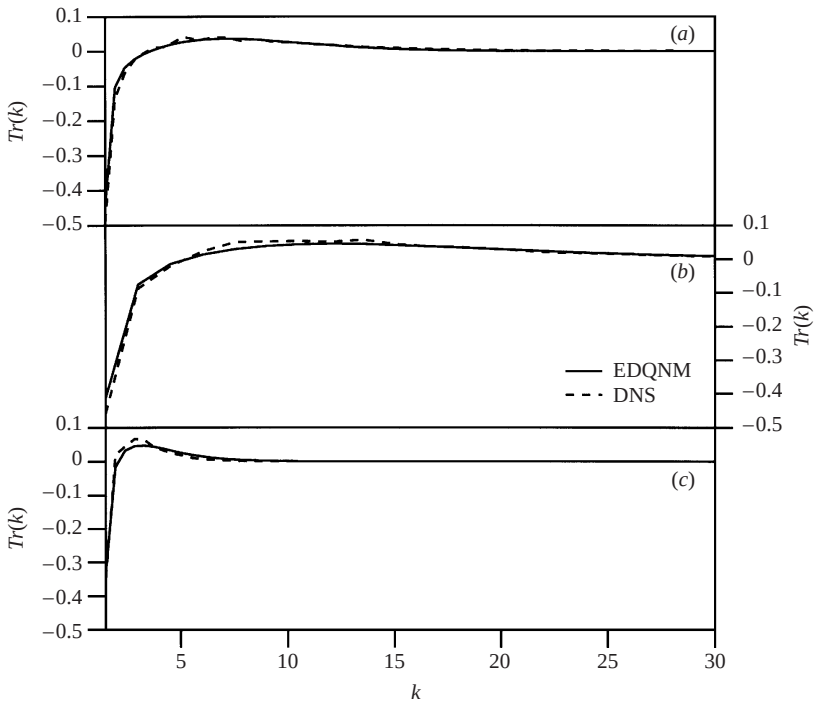

FIGURE 28. Total transfer function versus wavenumber at Schmidt numbers of (*a*) 1, (*b*) $\frac{1}{4}$ and (*c*) $\frac{1}{16}$.

The good agreement between the model and simulations motivated us to use the model to look more closely at the scaling of differential diffusion with Reynolds number. The EDQNM model predicts $(1-\tilde{\rho}) \propto Re_\lambda^{-1}$, in agreement with the scaling argument put forth by Kerstein *et al.* (1995) for $\overline{z'^2}$. Moreover, we showed that the result can be reproduced from a simplified scalar spectrum containing an Oboukov–Corrsin inertial range followed by the Batchelor inertial–conductive range.

The scaling proposed by Yeung (1998), was shown to collapse the spectra $E_z(k/k_\alpha)$ and $\rho(k\eta)$ onto a single curve, independent of the value of the Reynolds number (note that species α is assumed to be the more slowly diffusing species). This remarkable result implies an important reduction in the parameter space. However, the further reduction of $\rho(k\eta)$ into a Schmidt-number-dependent function and a wavenumber-dependent function was not supported by the EDQNM results. Instead, an intermediate result is achieved that allows the elimination of the dependence on the Reynolds number, but requires a more complicated functional dependence on the two Schmidt numbers.

Local versus non-local transfer was investigated by decomposing the energy spectrum in the transfer function into three different ranges of wavenumbers. The results indicate that scalar transfer is dominated first by local interactions (local transfer), followed by non-local interactions that lead to local transfer. Non-local interactions that lead to non-local transfer are significant only at high wavenumbers. A comparison of the different spectral interactions in the transfer function showed that *RB* interactions were dominant over the entire spectrum. Both of these results have important implications for developing simpler spectral models. For example, local and non-local interactions leading to predominantly local transfer implies that the com-

putationally expensive convolution integrals in the EDQNM model can be simplified. Additionally, the dominanance of *RB* interactions suggests that the other interactions can be neglected, thereby further reducing the cost of the calculation.

Finally, our EDQNM calculations of the backscatter coefficient β_D, defined by Fox (1999) to account for the inverse cascade of incoherence in his model, were shown not to capture the Schmidt number dependence found in the DNS. The standard (unrealizable) EDQNM model does a better job. This suggests that the modifications of the EDQNM model, required to fix the realizability problem, have compromised the model's prediction of the split between forward and reverse transfer. It should be emphasized that a self-consistent EDQNM model for the covariance spectrum cannot be obtained without altering the autocorrelation spectrum in the manner suggested by UC. Nevertheless, it is encouraging that the total transfer spectrum continues to show excellent agreement with DNS over a broad range of Schmidt numbers.

Support for M. U. was provided by the United States Department of Energy Accelerated Strategic Computing Initiative (ASCI) program and Los Alamos National Laboratory, Group T-3. Support for T. V. and L. R. C. was provided by the National Science Foundation Grant CTS-9732223. All numerical simulations were performed on IBM SP2 nodes that were provided by a grant from the IBM Shared University Research (SUR) program.

REFERENCES

André, J. C. & Lesieur, M. 1977 Influence of helicity on the evolution of isotropic turbulence at high Reynolds number. *J. Fluid Mech.* **81**, 187.

Batchelor, G. K. 1946 The theory of axisymmetric turbulence. *Proc. R. Soc. Lond.* A **186**, 480.

Batchelor, G. K., Howells, I. D. & Townsend, A. A. 1959 Small-scale variation of convected quantities like temperature in a turbulent fluid. Part 2. The case of large conductivity. *J. Fluid Mech.* **5**, 134–139.

Besnard, D. C., Harlow, F. H., Rauenzahn, R. M. & Zemach, C. 1996 Spectral transport model for turbulence. *Theor. Comput. Fluid Dyn.* **8**, 1.

Bilger, R. W. & Dibble, R. W. 1982 Differential molecular diffusion effects in turbulent mixing. *Combust. Sci. Tech.* **28**, 161.

Brasseur, J. G. & Wei, C.-H. 1994 Interscale dynamics and local isotropy in high Reynolds number turbulence. *Phys. Fluids* **6**, 842.

Chandrasekhar, S. 1950 The decay of axisymmetric turbulence. *Phil. Trans. R. Soc. Lond.* A **242**, 557.

Chen, J.-Y., Bilger, R. W. & Dibble, R. W. 1990 Pdf modeling of nonpremixed $CO/H_2/N_2$ jet flames with reduced mechanisms. In *Twenty-third Sym.* (*Intl*) *on Combustion*, Pittsburgh. The Combustion Institute.

Clark, T. T. & Zemach, C. 1998 Symmetries and the approach to statistical equilibrium in isotropic turbulence. *Phys. Fluids* **10**, 2846–2858.

Domaradzki, J. A. & Rogallo, R. S. 1990 Local energy transfer and nonlocal interactions in homogeneous, isotropic turbulence. *Phys. Fluids* A **2**, 413.

Drake, M. C., Pitz, R. W. & Lapp, M. 1986 Laser measurements on nonpremixed H_2–air flames for assessments of turbulent combustion models. *AIAA J.* **24**, 905.

Eswaran, V. & Pope, S. B. 1988 An examination of forcing in direct numerical simulations of turbulence. *Comput. Fluids* **16**, 257.

Fox, R. O. 1992 The Fokker–Planck closure for turbulent molecular mixing: passive scalars. *Phys. Fluids* A **4**, 1230–1244.

Fox, R. O. 1995 The spectral relaxation model of the scalar dissipation rate in homogeneous turbulence. *Phys. Fluids* **7**, 1082.

Fox, R. O. 1997 The Lagrangian spectral relaxation model of the scalar dissipation in homogeneous turbulence. *Phys. Fluids* **9**, 2364.

Fox, R. O. 1999 The Lagrangian spectral relaxation model for differential diffusion in homogeneous turbulence. *Phys. Fluids* **11**, 1550–1571.

Fox, R. O. & Yeung, P.-K. 1999 Forward and backward spectral transfer in the modeling of scalar mixing in homogeneous turbulence. In *Third ASME/JSME Joint Fluids Engng Conf.*

Girimaji, S. S. 1991 Assumed β-pdf model for turbulent mixing: validation and extension to multiple scalar mixing. *Combust. Sci. Tech.* **78**, 177.

Girimaji, S. S. 1992 On the modeling of scalar diffusion in isotropic turbulence. *Phys. Fluids* A **4**, 2529.

Herr, S., Wang, L.-P. & Collins, L. R. 1996 EDQNM model of a passive scalar with a uniform mean gradient. *Phys. Fluids* **8**, 1588–1608.

Herring, J. R. 1974 Approach of axisymmetric turbulence to isotropy. *Phys. Fluids* **17**, 859.

Herring, J. R., Schertzer, D., Lesieur, M., Newman, G. R., Chollet, J. P. & Larcheveque, M. 1982 A comparative assessment of spectral closures as applied to passive scalar diffusion. *J. Fluid Mech.* **124**, 411.

Hinze, J. O. 1975 *Turbulence*. McGraw-Hill, New York.

Jaberi, F. A., Miller, R. S., Mashayek, F. & Givi, P. 1997 Differential diffusion in binary scalar mixing and reaction. *Combust. Flame* **109**, 561–577.

Kerstein, A. R., Cremer, M. A. & McMurtry, P. A. 1995 Scaling properties of differential molecular effects in turbulence. *Phys. Fluids* **7**, 1999.

Kerstein, A. R., Dibble, R. W., Long, M. B., Yip, B. & Lyons, K. 1989 Measurement and computation of differential molecular diffusion in a turbulent jet. In *Seventh Symp. on Turbulent Shear Flows*, paper 14–2.

Leith, C. E. 1967 Diffusion approximation to inertial energy transfer in isotropic turbulence. *Phys. Fluids* **10**, 1409.

Lesieur, M. 1987 *Turbulence in Fluids, Stochastic and Numerical Modeling*. M. Nijhoff, Boston.

Lesieur, M. & Schertzer, D. 1978 Amortissement auto similaire d'une turbulence à grand nombre de Reynolds. *J. Méc* **17**, 609.

Millionshtchikov, M. 1941 On the theory of homogeneous isotropic turbulence. *Dokl. Akad. Nauk. SSSR* **32**, 615.

Nakauchi, N., Oshima, H. & Saito, Y. 1989 A passive scalar convected by homogeneous axisymmetric turbulence. *Phys. Fluids* A **1**, 723.

Nilsen, V. & Kosály, G. 1997 Differential diffusing scalars in turbulence. *Phys. Fluids* **9**, 3386–3397.

Nilsen, V. & Kosály, G. 1999 Differential diffusion in turbulent reacting flows. *Combust. Flame* **117**, 493–513.

O'Brien, E. E. & Francis, G. C. 1962 A consequence of the zero fourth cumulant approximation. *J. Fluid Mech.* **13**, 369–382.

Ogura, Y. 1963 A consequence of the zero-fourth-cumulant approximation in the decay of isotropic turbulence. *J. Fluid Mech.* **16**, 33–40.

Orszag, S. A. 1970 Analytical theories of turbulence. *J. Fluid Mech.* **41**, 363–386.

Pope, S. B. 1985 Pdf methods for turbulent reactive flows. *Prog. Energy Combust. Sci.* **11**, 119–192.

Pope, S. B. 2000 *Turbulent Flows* Cambridge University Press. p. 232.

Pouquet, A., Lesieur, M., Andre, J. C. & Basdevant, C. 1975 Evolution of high Reynolds number two-dimensional turbulence. *J. Fluid Mech.* **72**, 305.

Saylor, J. R. & Sreenivasan, K. R. 1998 Differential diffusion in low Reynolds number water jets. *Phys. Fluids* **10**, 1135–1146.

Smith, L. L., Dibble, R. W., Talbot, L., Barlow, R. S. & Carter, C. D. 1995*a* Laser raman scattering measurements of differential molecular diffusion in nonreacting turbulent jets of H_2/CO_2 mixing with air. *Phys. Fluids* **7**, 1455–1466.

Smith, L. L., Dibble, R. W., Talbot, L., Barlow, R. S. & Carter, C. D. 1995*b* Laser raman scattering measurements of differential molecular diffusion in turbulent nonpremixed jet flames of H_2/CO_2 fuel. *Combust. Flame* **100**, 153–160.

Ulitsky, M. & Collins, L. R. 2000 On constructing realizable, conservative mixed scalar equations using the eddy damped quasi-normal markovian theory. *J. Fluid Mech.* **412**, 303–329 (referred to herein as UC).

Vedula, P., Yeung, P.-K. & Fox, R. O. 2001 Dynamics of scalar dissipation in isotropic turbulence: a numerical and modeling study. *J. Fluid Mech.* **433**, 29–60.

Vignon, J.-M. & Cambon, C. 1980 Thermal spectral calculation using eddy-damped quasi-normal markovian theory. *Phys. Fluids* **23**, 1935–1937.

Vranos, A., Knight, B. A., Proscia, W. M., Chiappetta, L. & Smooke, M. D. 1992 Nitric oxide formation and differential diffusion in a turbulent methane–hydrogen diffusion flame. In *Twenty-fourth Symp.* (*Intl*) *on Combustion*, Pittsburgh. The Combustion Institute.

Williams, F. A. 1985 *Combustion Theory*. Addison-Wesley.

Yeung, P. K. 1996 Multi-scalar triadic interactions in differential diffusion with and without mean scalar gradients. *J. Fluid Mech.* **321**, 235–378.

Yeung, P. K. 1998 Correlations and conditional statistics in differential diffusion: scalars with uniform mean gradients. *Phys. Fluids* **10**, 2621–2635.

Yeung, P. K. & Pope, S. B. 1993 Differential diffusion of passive scalars in isotropic turbulence. *Phys. Fluids* A **5**, 2467.

Zhou, Y. 1993*a* Degrees of locality of energy transfer in the inertial range. *Phys. Fluids* A **5**, 1092–1094.

Zhou, Y. 1993*b* Interacting scales and energy transfer in isotropic turbulence. *Phys. Fluids* A **5**, 2511–2524.